Journal of Materials Chemistry A

REVIEW

View Article Online
View Journal | View Issue

Cite this: J. Mater. Chem. A, 2023, 11, 12539

Highly selective semiconductor photocatalysis for CO_2 reduction

Shan Yao,[ab] Jiaqing He,[ab] Feng Gao,[ab] Haowei Wang,[ab] Jiahui Lin,[ab] Yang Bai,[ab] Jingyun Fang,[c] Feng Zhu,[e] Feng Huang[abd] and Mengye Wang *[ab]

Received 27th November 2022
Accepted 6th January 2023

DOI: 10.1039/d2ta09234d

rsc.li/materials-a

Over the past few decades, photocatalytic CO_2 reduction has remained a prominent and growing research field due to the efficient conversion of CO_2 to value-added chemicals. Among the various photocatalytic performances, product selectivity has garnered considerable attention, which is the focus of this review. Herein, we first introduce the general background of photocatalytic CO_2 reduction, then according to the sequence of the entire reaction process, the adsorption and activation of reactants, the formation and stabilization of intermediates, and the desorption of products are summarized. After introducing each of the above steps that could mediate the final products, several modification techniques to improve the product selectivity are highlighted, including noble metal decoration, metal and non-metal doping, vacancy engineering, facet engineering, composite construction, and hydroxyl modification. Finally, current challenges and opportunities of interest in this rich field are discussed.

10th anniversary statement

Journal of Materials Chemistry A is one of the most important journals that concentrates on material applications in energy and sustainability and covers a wide range of specific content. In past studies, we focused on advanced materials for photocatalysis, piezocatalysis and electrocatalysis, including hydrogen production, nitrogen fixation, CO_2 reduction and degradation of organic pollutants. Our research interests include designing efficient catalysts *via* morphology control, vacancy engineering, size adjustment and modification. The source of synthetic reagents can be either chemical reagents or solid waste. Making solid waste into catalysts can alleviate the environmental problems caused by waste residue disposal sites. Moreover, we also concentrate on the catalytic mechanism using advanced spectroscopic techniques. On the occasion of the tenth anniversary of *Journal of Materials Chemistry A*, we sincerely celebrate the 10th anniversary of *Journal of Materials Chemistry A* and look forward to making further progress with the development of the journal in the future.

[a]*School of Materials, Sun Yat-Sen University, Shenzhen 518107, China. E-mail: wangmengye@mail.sysu.edu.cn*

[b]*State Key Laboratory of Optoelectronic Materials and Technologies, Sun Yat-Sen University, Guangzhou 510275, China*

[c]*Guangdong Provincial Key Laboratory of Environmental Pollution Control and Remediation Technology, School of Environmental Science and Engineering, Sun Yat-Sen University, Guangzhou 510275, China*

[d]*Ganjiang Innovation Academy, Chinese Academy of Sciences, Ganzhou 341000, PR China*

[e]*Shenzhen Shiage Electronic Technology Co., Ltd, Shenzhen 518107, China*

Shan Yao received her B.E. in polymer materials and engineering from Guangdong University of Technology. She is currently pursuing her PhD under the supervision of Prof. Mengye Wang in the School of Materials at Sun Yat-Sen University. Her current research focuses on advanced materials for photocatalysis and environmental applications.

Jiaqing He received her B.S. degree from Sun Yat-sen University. She is currently pursuing her PhD under the supervision of Prof. Mengye Wang in Sun Yat-sen University. Her current research focuses on advanced materials for piezocatalysis and environmental applications.

1. Introduction

The industrial revolution has triggered the rapid development of science and technology,[1–10] however, the massive consumption of fossil fuels has caused a sharp increase in CO_2 concentration.[11–17] As of December 2020, CO_2 concentration in the atmosphere has reached 414.02 ppm, far higher than 270 ppm in the early 1800s, which is considerably higher than the safe value of atmospheric CO_2 concentration (*i.e.*, 350 ppm).[18] As a consequence, a series of natural disasters, such as desertification, global warming and ocean acidification, have occurred frequently.[19–21] Therefore, it has become an urgent issue to both alleviate the pollution caused by CO_2 and replace fossil fuels with clean and renewable energy sources.[22–28]

The photocatalytic conversion of CO_2 into hydrocarbon fuels of small molecular weight, such as CH_4, CH_3OH and C_2H_5OH, might kill two birds with one stone in terms of protecting the environment and saving energy.[29–32] In the past several decades, tremendous efforts have been made toward CO_2 reduction initiated by solar light,[33–38] and thus far, the activity of photocatalytic CO_2 reduction has greatly improved. Although the research and reports on the regulation of photocatalytic activity have been quite thorough, CO_2 reduction still has an obvious drawback, which is low selectivity and can be mainly attributed to the following reasons. First, as the energy barrier of CO_2 reduction to target products is comparable to that of hydrogen evolution (eqn (1)–(7) at pH 7 in aqueous solution), the side reaction (*i.e.*, hydrogen generation) is inevitable.[39,40]

$$CO_2 + 2H^+ + 2e \rightarrow CO + H_2O \quad E^0 = -0.52 \text{ V } \textit{vs.} \text{ NHE} \quad (1)$$

$$CO_2 + 2H^+ + 2e \rightarrow HCOOH \quad E^0 = -0.61 \text{ V } \textit{vs.} \text{ NHE} \quad (2)$$

$$CO_2 + 4H^+ + 4e \rightarrow HCHO + H_2O \quad E^0 = -0.51 \text{ V } \textit{vs.} \text{ NHE} \quad (3)$$

$$CO_2 + 8H^+ + 8e \rightarrow CH_4 + 2H_2O \quad E^0 = -0.24 \text{ V } \textit{vs.} \text{ NHE} \quad (4)$$

$$CO_2 + 6H^+ + 6e \rightarrow CH_3OH + H_2O \quad E^0 = -0.38 \text{ V } \textit{vs.} \text{ NHE} \quad (5)$$

$$CO_2 + 12H^+ + 12e \rightarrow C_2H_4 + 4H_2O \quad E^0 = -0.34 \text{ V } \textit{vs.} \text{ NHE} \quad (6)$$

$$2H^+ + 2e \rightarrow H_2 \quad E^0 = -0.42 \text{ V } \textit{vs.} \text{ NHE} \quad (7)$$

Thus, CO_2 reduction exhibits limited selectivity in aqueous solutions due to the critical challenge of overcoming the competition with the hydrogen evolution reaction (HER). In addition, the reduction potentials of converting CO_2 to different products are similar (eqn (1)–(6)).[41] This phenomenon results in an undesirable mixture of products, which is hard to separate and utilize. Therefore, the improvement in selectivity is of key importance for photocatalytic CO_2 reduction.[42–45]

This review aims to summarize recent impressive developments in the highly selective photocatalytic CO_2 reduction. After a brief discussion that motivates the research on high product selectivity, the reaction mechanism of photocatalytic CO_2 reduction is introduced to better understand the obstacle of reaction selectivity and the specific steps involved in the entire photocatalytic procedure. Then, the promotion of selective reaction at different reaction stages is summarized, including the adsorption and activation of reactants (*i.e.*, CO_2 adsorption

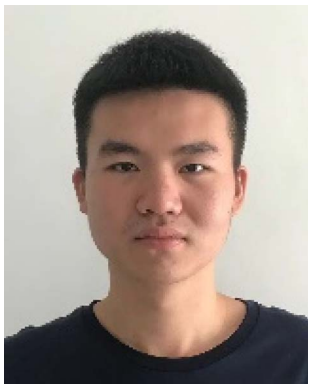

Feng Gao received his B.S. degree from Sun Yat-Sen University. He is currently pursuing his PhD under the supervision of Prof. Mengye Wang in Sun Yat-Sen University. His current research focuses on advanced materials for electrocatalysis and energy-related applications.

Haowei Wang is pursuing his master's degree in the school of materials at Sun Yat-Sen University. He obtained his B.E. in polymer materials and engineering from Wuhan University of Technology in 2021. His current research focuses on advanced materials for electrocatalysis.

Jiahui Lin is pursuing her PhD in the School of Materials at Sun Yat-Sen University. She obtained her B.S. degree from Sun Yat-Sen University in 2022. Her current research focuses on advanced materials for electrocatalysis and environmental applications.

Mengye Wang is an Associate Professor in the School of Materials at Sun Yat-Sen University. She received her PhD in Physical Chemistry from Xiamen University. Her research interests include advanced materials for environmental and energy-related applications.

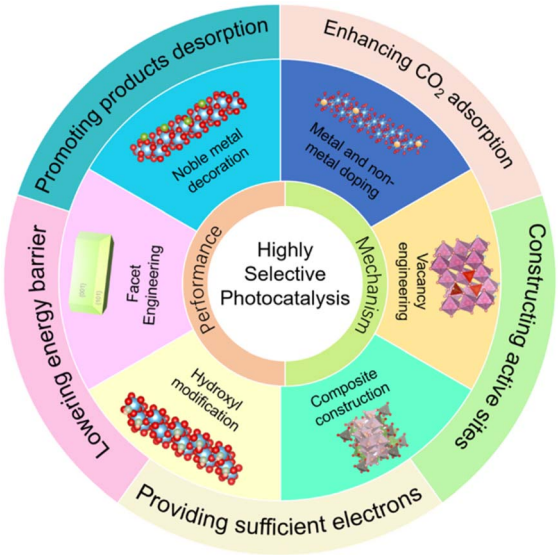

Fig. 1 Schematic illustration of photocatalyst modification and mechanisms in this review.

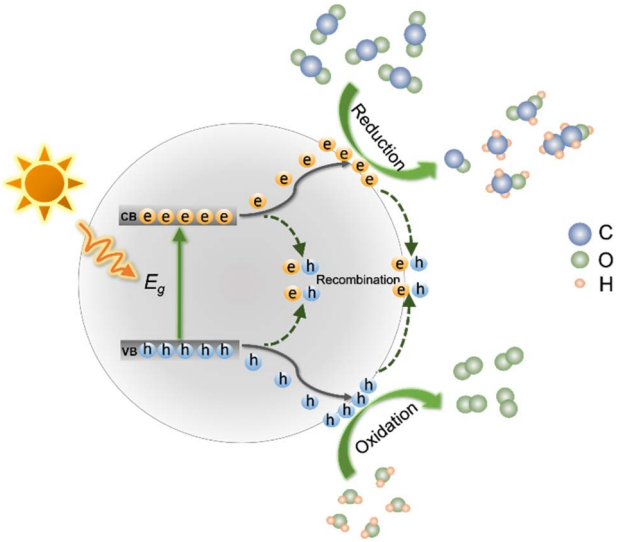

Fig. 2 Schematic illustration of photocatalytic CO_2 reduction.

[1]and H_2 evolution inhibition, electron supply and others), the formation and stabilization of intermediates (*i.e.*, the formation energy of crucial intermediates and stability of intermediates), and the desorption of products. Particularly, modification methods of photocatalysts to boost selective reactions are discussed, including noble metal decoration, metal and non-metal doping, vacancy engineering, facet engineering, composite construction, hydroxyl and ion modification and other decoration techniques (Fig. 1). Lastly, a perspective on the challenges and future research directions of photocatalytic CO_2 reduction possessing enhanced photocatalytic selectivity is proposed.

2. Mechanism of photocatalytic CO_2 reduction

Specific reaction processes of photocatalytic CO_2 reduction are displayed in Fig. 2. Under light irradiation, the semiconductor photocatalyst absorbs photons. If the photon energy is equal to or larger than the band gap (E_g) of the photocatalyst, electrons and holes of the semiconductor are generated. The photogenerated electrons and holes then migrate to the surface of the photocatalyst.[46] Photogenerated electrons are capable of reduction reactions that reduce CO_2 on the surface of the semiconductor be reduced, while the holes oxidize H_2O to O_2. Photo-excited electrons and holes are prone to recombine both during the migration to photocatalyst surface and after reaching the surface, which significantly reduces the photocatalytic efficiency. Some parameters affect the reaction selectivity, including the reduction potentials of CO_2 to products, the adsorption and desorption of different substances (*i.e.*, CO_2, intermediates and products), and the utilization efficiency of photogenerated electrons.

The standard reduction potentials of CO_2 are summarized in eqn (1)–(6) and eqn (8).[47] As shown in eqn (8), $CO_2^{\bullet-}$ formation through the single-electron reduction of CO_2 is unfavorable due to its very negative redox potential (*i.e.*, −1.90 V *vs.* NHE).

$$CO_2 + e^- \rightarrow CO_2^{\bullet-} \quad E^0 = -1.90 \text{ V } vs. \text{ NHE} \tag{8}$$

Therefore, multi-proton-assisted CO_2 reduction reactions are prone to occur, possessing a relatively low thermodynamic barrier and bypassing the formation of $CO_2^{\bullet-}$ (eqn (1)–(6)).[48] From a thermodynamic point of view, the potentials of CO_2 reduction (eqn (1)–(6)) are comparable to the potentials of hydrogen evolution (eqn (7)), which leads to a large amount of H_2 as the by-product.[49] According to the less negative redox potentials, it seems that the photoconversion of CO_2 to CH_3OH and CH_4 is more favorable than the H_2 evolution ([eqn (4)], [eqn (5)] and [eqn (7)]). Nevertheless, the requirement of more electrons to accomplish highly selective formation of CH_3OH and/or CH_4 rather than H_2 is a great challenge.[50] Therefore, in order to realize the highly selective photoconversion of CO_2, the photocatalysts should be carefully designed to suppress H_2 evolution. In addition to the interference of H_2, the small differences between the thermodynamic potentials of different CO_2 reduction products also make it tough to obtain single desirable products.[40]

Typically, the photocatalytic CO_2 reduction process involves three major steps: (i) the chemical capture and adsorption of CO_2 on the surface of the photocatalyst; (ii) activation and breaking of C–O bonds and the formation of C–H bonds *via* electron transfer and proton migration; (iii) the configuration rearrangement of products and desorption from the photocatalysts.[51] Each reaction step can be regulated by modifying photocatalysts or reaction conditions. In step (i), if the CO_2 adsorption is enhanced and H_2O adsorption is inhibited, the efficiency of CO_2 reduction will be largely increased and the H_2 evolution will be reduced.[52] Similarly, in step (ii), to obtain the products such as CH_4, CH_3OH and C_2H_4, a mass of electrons is needed. Thus, a sufficient electron supply and proper

suppression of electron–hole recombination are beneficial for their generation.[53] During the configuration rearrangement and intermediate conversion process, the formation and stabilization of crucial intermediates determine the direction of the subsequent reactions, promoting the selective generation of the target products. Finally, the easy desorption of obtained products can further enhance the selectivity.

3. Typical methods to enhance the selectivity and mechanism

Diverse strategies, including noble metal decoration, metal and non-metal doping, vacancy engineering, the exposure of highly active crystal facets, construction of complex materials, surface modification, morphology control and other methods, have been explored to manipulate the selectivity of the photocatalytic CO_2 reduction. These techniques significantly increase the selectivity in terms of kinetics, adsorption and desorption capacity, electron supply, and intermediate stability. Diverse modification methods will affect different steps of CO_2 reduction. Oxygen vacancies, noble metal and non-metal particles can not only affect the adsorption of CO_2 but can also act as electron sinks, providing sufficient electrons for products. Composite construction, which can improve the CO_2 capture capability, also facilitates efficient photo-excited electron transfer and accumulation. Morphology control and facet engineering mainly affect the adsorption and desorption process during CO_2 reduction. We will introduce typical methods in the following sections. However, most of the work only briefly explains the reasons for the improvement of selectivity, rarely involving the essential reasons. The modified highly selective photocatalysts are listed in Table 1.

3.1. Adsorption and activation of reactants

3.1.1. CO_2 adsorption and H_2 evolution inhibition. As mentioned in Section 2, the hydrogen evolution is one of the main competing reactions for CO_2 reduction, which could remarkably decrease the efficiency and selectivity of CO_2 reduction.[49,80] Therefore, whether the catalysts tend to capture CO_2 molecules or H_2O and whether electrons tend to combine with CO_2, H^+ or hydroxy groups from water molecules significantly affect the final products.[46] As a consequence, CO_2 adsorption is crucial to improve the selectivity. Here, we have summarized some special sites, including noble metal particles, oxygen vacancies and hydroxyl groups, which can effectively adsorb CO_2 molecules and initiate rapid CO_2 reduction reactions.[46,72,81,82] Moreover, on exposing expected crystal planes and constructing composite structures, active sites can be provided for the preferential adsorption and conversion of CO_2 molecules, suppressing the H_2 generation.[83]

For example, nearly 100% selective CO generation was achieved on the surface of spindle-like oxygen-vacancy rich (V_O-rich) Pt–Ga_2O_3 (Fig. 3a).[81] The oxygen vacancies served as the main sites for CO_2 adsorption.[81] Meanwhile, the hydrogen formed on Pt nanoparticles in the process of photocatalytic water splitting could quickly reduce the adsorbed CO_2.[81] Besides Pt, other noble metals also showed similar effects. After anchoring Au–Pd alloy on the {101}*n* facets of TiO_2, the Au–Pd alloy provided abundant sites for CO_2 adsorption and activation.[73] Remarkably, the optimal sample achieved a high selectivity of 85% for hydrocarbons (71%: CH_4, 14%: C_2H_4 and C_2H_6, Fig. 3b).[73]

Some special groups are also capable of the adsorption and activation of CO_2. For instance, the –OH groups on the Cu_2O surface facilitated the selective catalytic CO_2 reduction by suppressing the hydrogen evolution.[84] Besides, in the noble-metal-free SiO_2–TiO_2 system, the enhanced CO_2 photoreduction selectivity was assigned to the rational hydrophobic modification of the TiO_2–SiO_2 surface by replacing Si–OH with hydrophobic Si–F bonds.[85] This kind of modification changed the hydrophilicity and hydrophobicity of the photocatalyst surface and thus mediated the reaction process.[85] This improved selectivity was attributed to the efficient CO_2 adsorption, triggering efficient CO_2 photoreduction.[85]

Different crystal faces possess different CO_2 adsorption capacities.[86] ZnO nanomaterials with a large ratio of {0001} facets could enhance the CO production selectivity and the exposed facets were terminated with a high density of oxygen atoms.[87] Therefore, oxygen vacancies were prone to form on the surface of ZnO.[87] These vacancies could preferentially capture CO_2 molecules and work as reduction sites for CO_2.[87] As a consequence, the CO molecules could be produced as the main products.[87] In addition, BiOBr nanosheets exposing {001} facets were successfully synthesized in the presence of nitric acid.[83] Compared to the BiOBr nanosheets prepared in the absence of nitric acid (BiOBr-0), the {001} facets-dominated BiOBr nanosheets exhibited more efficient CO_2 absorption and activation, selectively converting CO_2 to CO (Fig. 3c).[83]

The adsorption and activation capacity can also be improved by changing the structure of the material. Typically, g-C_3N_4-based composite catalysts display strong CO_2 capture ability, which promotes the generation of CO rather than H_2.[88]

The selectivity enhancement of CO production also appeared in other semiconductor composites, such as LDH/Ti_3C_2 and Ga_2O_3/$ZnGa_2O_4$.[46,67] Taking the Ga_2O_3/$ZnGa_2O_4$ catalyst as an example, the $ZnGa_2O_4$ layer could suppress the reduction of H^+.[67] The proposed mechanism is displayed in Fig. 3d. Since a large number of active sites on the surface of Ga_2O_3 could capture and reduce H^+, the main reaction on the surface of Ag–Ga_2O_3 was hydrogen production (Fig. 3d).[67] After the growth of the $ZnGa_2O_4$ layer on the surface of Ga_2O_3, it blocked the active sites that are conducive to hydrogen evolution. Therefore, with the amount of $ZnGa_2O_4$ increasing from 0.1 to 10.0 mol%, the generation of H_2 was significantly suppressed. Finally, CO generation with nearly 100% selectivity was achieved over Ga_2O_3/$ZnGa_2O_4$ heterostructures (Fig. 3e).[67] Crafting ultrathin two-dimensional semiconductor nanomaterials is another popular technique for achieving high photocatalytic selectivity.[89–92] Bai found that compared with the bulk counterpart, the ultrathin $Bi_4O_5Br_2$ ($Bi_4O_5Br_2$-UN) exhibited increased CO generation of over 99.5% through an enhanced CO_2 adsorption capacity (Fig. 3f).[72]

Table 1 Summary of highly selective photocatalysts for CO_2 reduction

Photocatalyst	Light source	Experimental conditions	Main products and selectivity	Ref.
$Ag/CaTiO_3$	100 W Hg lamp	0.3 g of catalysts, $NaHCO_3$ aqueous solution (1.0 M)	CO (180 μmol g^{-1} h^{-1}), 94%	54
TiO_2–Pd@Au	300 W Xe lamp	15 mg of catalysts, CO_2 and 5 mL H_2O	CH_4 (48.2 μmol g^{-1} h^{-1}), 93.5%	55
(Pt/TiO_2)@rGO	300 W Xe lamp	Certain amounts of catalysts, CO_2 and 2 mL H_2O	CH_4 (41.3 μmol g^{-1} h^{-1}), 99.1%	56
Pt@Ag–TiO_2	350 W Xe lamp	Certain amounts of catalysts, CO_2 and Na_2SO_4 aqueous solution (0.5 M)	CH_4 (160.3 μmol g^{-1} h^{-1}), 87.9%	57
Pt/TiO_2	300 W Xe lamp	50 mg of catalysts, CO_2 and 50 mL H_2O	CH_4 (150.04 μmol g^{-1} h^{-1}), nearly 100%	58
N-doped C dot/CoAl-LDH/C_3N_4	300 W Xe lamp	50 mg of catalysts, CO_2 and 300 μL H_2O	CH_4 (25.69 μmol g^{-1} h^{-1}), 99%	59
N–TiO_2	200 W Hg lamp	Gas mixture of CO_2 and H_2 with a ratio of 1 : 1	CO (56.30 μmol g^{-1} h^{-1}), 96.3%	60
Cu–TiO_2	300 W Xe lamp	60 mg of catalysts, 1.60 g $NaHCO_3$ and 5 mL H_2SO_4 solution (5.0 M)	CH_4 (150.9 μmol g^{-1} h^{-1}), 85%	61
WO_{3-x}	UV-Vis-NIR light	5 mg of catalysts, CO_2 and 0.2 mL H_2O	C_2H_4 (61.6 μmol g^{-1} h^{-1}), 89.3%	62
$BiMoO_6$	300 W Xe lamp	50 mg of catalysts, 1.50 g $NaHCO_3$ and 5 mL H_2SO_4 (4 M)	CH_4 (2.01 μmol g^{-1} h^{-1}), 96.7%	63
Defective CeO_2	300 W Xe lamp	50 mg of catalysts, CO_2 and 0.2 mL H_2O	CO (7 μmol g^{-1} h^{-1}), nearly 100%	64
g-C_3N_4/$FeWO_4$	Visible light (λ > 420 nm)	40 mg of catalysts, CO_2 and H_2O	CO (6 μmol g^{-1} h^{-1}), 99%	65
NiAl-LDH/Ti_3C_2	300 W Xe lamp	100 mg of catalysts, CO_2 and 0.4 mL H_2O	CO (11.82 μmol g^{-1} h^{-1}), 92%	66
Ag-loaded Ga_2O_3/$ZnGa_2O_4$	400 W Hg lamp	1 g of catalysts, CO_2 and 1 L H_2O	CO, nearly 100%	67
Pt/HAP/TiO_2	300 W Xe lamp	20 mg of catalysts, CO_2 and 40 mL H_2O	CH_4 (4.64 μmol g^{-1} h^{-1}), 99.1%	68
C_3N_4/$Pd_9Cu_1H_x$	Visible light	15 mg of catalysts, CO_2 and H_2O	CH_4 (1.20 μmol g^{-1} h^{-1}), nearly 100%	69
Cl^-/Bi_2WO_6	300 W Xe lamp	20 mg of catalysts, CO_2 and H_2O	CH_4 (3.21 μmol g^{-1} h^{-1}), 94.98%	70
Pt@h-BN	300 W Xe lamp	10 mg of catalysts, CO_2 and 0.5 mL H_2O	CH_4 (184.7 μmol $g_{(Pt)}^{-1}$ h^{-1}), 99.1%	71
Ultrathin $Bi_4O_5Br_2$	300 W Xe lamp	20 mg of catalysts, CO_2 and H_2O	CO (31.565 μmol g^{-1} h^{-1}), 99.5%	72
Au–Pd alloying loaded TiO_2	UV light	10 mg of catalysts, CO_2 and H_2O	Hydrocarbon fuels (CH_4, C_2H_4, and C_2H_6) (25.06 μmol g^{-1} h^{-1}), 85%	73
V-defective $BiVO_4$	300 W Xe lamp	100 mg of catalysts, CO_2 and H_2O	CH_3OH (398.3 μmol g^{-1} h^{-1})	74
Defective C_3N_4	350 W Xe lamp	100 mg of catalysts, CO_2 and H_2O	CH_4, CH_3OH, and CH_3CH_2OH (12.07 μmol g^{-1} h^{-1}), 91.5%	75
W-doped g-C_3N_4	300 W Xe lamp	5 mg of catalysts, CO_2 and H_2O	CH_4 and C_2H_4 (11.91μmol g^{-1} h^{-1}), 83%	76
$Cu_xIn_5S_8$–Cu_ySe	300 W Xe lamp	10 mg of catalysts, CO_2 and H_2O	CH_3OH (5.25 μmol g^{-1} h^{-1}), about 100%	77
Microwave-synthesised carbon-dots	300 W Xe lamp	10 mg of catalysts, CO_2 and H_2O	CH_3OH (13.9 μmol g^{-1} h^{-1}), 99.6%	78
C_3N_4-supported CoS	300 W Xe lamp	10 mg of catalysts, CO_2 and H_2O	CH_3OH (97.3 μmol g^{-1} h^{-1}), 87.2%	79

In summary, by constructing composites, introducing metal sites and constructing oxygen vacancies, the adsorption and activation capabilities of photocatalysts in the first step of the CO_2 reduction reaction can be significantly improved. Therefore, the target reaction occurs instead of the competitive hydrogen evolution. However, in previous reports about the first

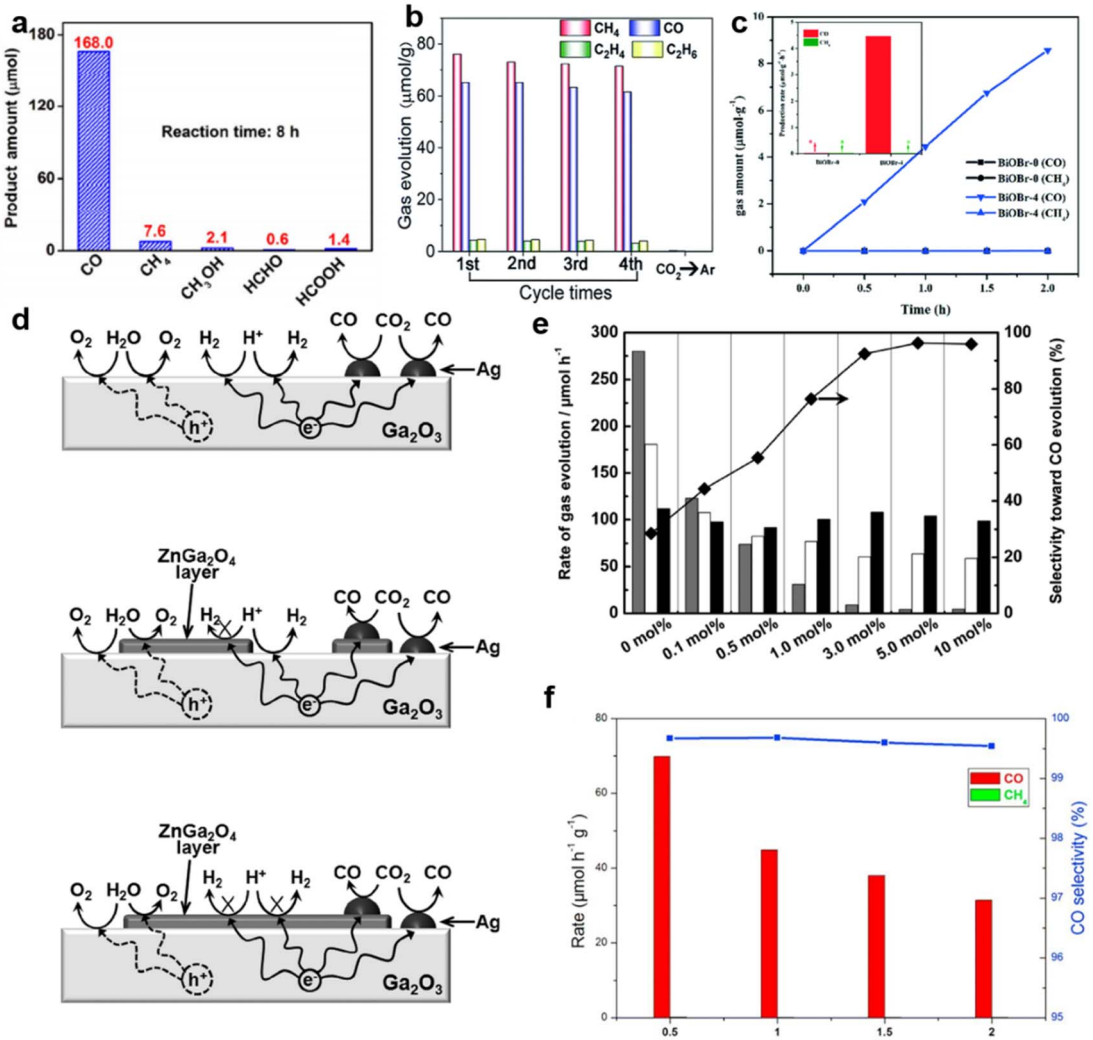

Fig. 3 (a) The amount of products over V_O-enriched Pt–Ga_2O_3 after irradiation for 8 h. Reproduced with permission from ref. 81 copyright 2018 Springer. (b) Photocatalytic yield and stability of Au–Pd-alloy-decorated TiO_2. Reproduced with permission from ref. 73. copyright 2019 Royal Society of Chemistry. (c) Production rates of CH_4 and CO over BiOBr photocatalysts under Xe light irradiation. Reproduced with permission from ref. 83 copyright 2017 Royal Society of Chemistry. (d) A proposed mechanism for the photocatalytic conversion of CO_2 in H_2O over Ag-loaded Ga_2O_3, Ag-loaded Zn-modified Ga_2O_3 with a low Zn content, and Ag-loaded Zn-modified Ga_2O_3 with a high Zn content. (e) Evolution rates of CO (black), O_2 (white), and H_2 (gray) in the photocatalytic conversion of CO_2 over Ag-loaded $ZnGa_2O_4$-modified Ga_2O_3 containing different amounts of $ZnGa_2O_4$. Reproduced with permission from ref. 67. Copyright 2016 Royal Society of Chemistry. (f) Evolution rates and selectivity over $Bi_4O_5Br_2$ and $Bi_4O_5Br_2$-UN under UV-vis illumination. Reproduced with permission from ref. 72. Copyright 2017 Elsevier.

step of the CO_2 reduction reaction, there is a lack of the selective generation of different carbon reduction products. In addition, how CO_2 adsorption mediates carbon products needs to be further explored.

3.1.2. Electron supply. The formation of high-value-added products such as CH_4 is usually a multi-electron reaction. In order to generate target products *via* multi-electron reactions, the accumulation of sufficient photogenerated electrons is necessary. Noble metals, non-metallic impurities and vacancies of photocatalysts can act as electron sinks, providing sufficient electrons for selective products.[53,57,93–96] Therefore, by constructing special nanostructures, electrons can be enriched in the target area to achieve selective reactions.

Pan *et al.* reported that after decoration by Pt nanoparticles, $LaPO_4$ reached a 5.6 times enhancement in CH_4 yield compared to pure $LaPO_4$ (Fig. 4a).[53] The selectivity of CH_4 production increased from the original 58.6% to 100% when the amount of modified Pt nanoparticles increased from 1 wt% to 3 wt% (Fig. 4a).[53] In this research, Pt nanoparticles functioned as the photogenerated electron sink, which thus accelerated the eight-electron reduction of CO_2 to CH_4.[53] This mechanism was proved in another report, where Pt/Cu_2O nanoparticles trapped sufficient photogenerated electrons and ensured the multielectron photocatalytic reactions to form CH_4 (Fig. 4b–d).[97] It is noteworthy that the electron sink effect of Pt also exists in other catalysts. The selectivity of CH_4 formation was improved when Pt@Ag core@shell structures were decorated on TiO_2

nanoparticles (Fig. 4e).[57] The Pt core served as a sink for photogenerated electrons, and the Ag shell suppressed the competitive photocatalytic water-splitting process. By tuning the ratio of Pt to Ag, 1.95 wt.‰ Pt@$Ag_{1.0}$–TiO_2 achieved the outstanding photocatalytic performance with a CH_4 formation rate of 160.3 mmol g^{-1} h^{-1} and a CO_2 conversion selectivity of 87.90%.[57]

Besides noble metals, doped common metals could also perform as electron traps and active sites for the highly selective CO_2 photoreduction.[104,105] For example, Cu doping effectively provided TiO_2 with electron traps, leading to a higher methanol yield.[93,106] The Cu sites of ZnO/CuO_x–C (the abbreviation C stands for Cu doping) carbon nanofibers (CNFs), which worked as electron traps, could also generate enough electrons for CH_4 formation (Fig. 4f).[99] Among ZnO–Cu_2O hybrid nanoparticles (ZnO@Cu_2O), Cu_2O cube–ZnO heterostructures (Cu_2O@ZnO), Cu_2O/ZnO nanocomposites (Cu_2O/ZnO) and Cu_2O/ZnO mixtures, ZnO/CuO_x–C CNFs demonstrated the highest CH_4 generation rate of 241.6 μmol h^{-1} g^{-1} with the selectivity of ~96% (Fig. 4g and h).[99] Besides the introduction of metallic Cu, highly selective CH_4 synthesis was achieved by introducing metal Mg.[100] CO_2 photoreduction rates of pure TiO_2 and TiO_2 decorated by different amounts of Mg are shown in Fig. 5a. Mg–TiO_2 promoted a large enhancement of electron trap sites, thereby ensuring sufficient electron supply for the selective reduction of CO_2 to CH_4.[100] Moreover, the doping or co-doping of other metals, such as Mo and Ce, could improve the photocatalytic conversion selectivity of CO_2 to high value-added products by increasing electron traps.[107,108] However, not all metals have the function of electron sink. Due to high CO_2 adsorption, In–TiO_2 nanoparticles achieved the highest CO selectivity of 94.39% with In doping of 10% (Fig. 5b) but with the limited electron supply, it was unable to achieve a high CH_4 yield.[101] Therefore, we need to select the appropriate metal to modify the photocatalyst according to the designed product target.[101]

The selective preparation of high-value-added products can be also achieved by creating oxygen vacancies.[111] Therefore,

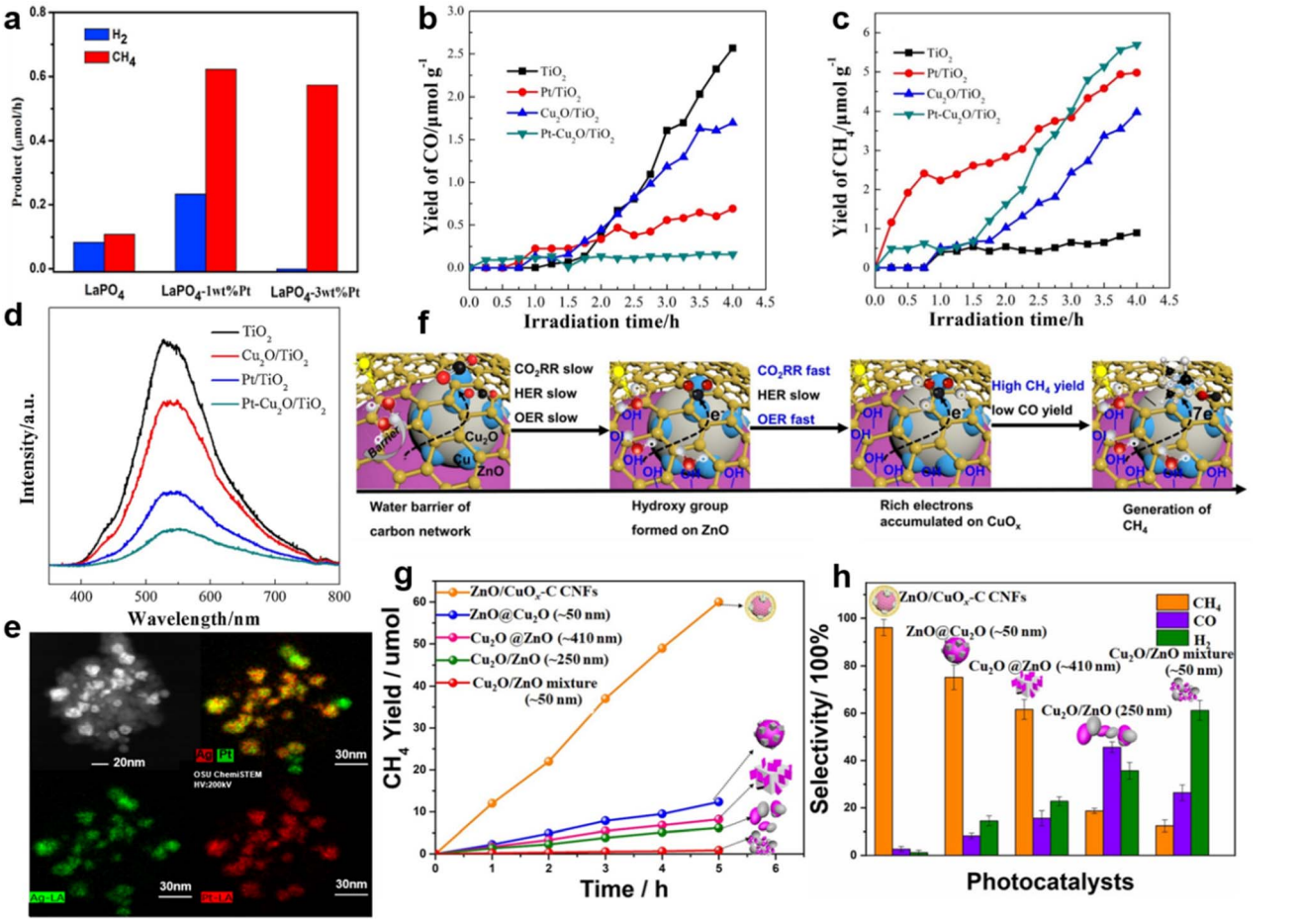

Fig. 4 (a) Generation rates of CH_4 and H_2 over the $LaPO_4$ and $LaPO_4$–Pt samples. Reproduced with permission from ref. 98 copyright 2015 Elsevier. (b) CO yields, (c) CH_4 yields and (d) PL spectra of TiO_2, Cu_2O/TiO_2, Pt/TiO_2 and Pt–Cu_2O/TiO_2. Reproduced with permission from ref. 97 copyright 2017 Elsevier. (e) STEM mapping images of Pt@$Ag_{1.0}$–TiO_2. Reproduced with permission from ref. 57 copyright 2018 Elsevier. (f) The proposed photocatalytic mechanism of highly selective CH_4 production over ZnO/CuO_x–C CNFs. (g) The CH_4 yield and (h) the product selectivity of ZnO/CuO_x–C CNFs, ZnO@CuO, Cu_2O@ZnO, ZnO/Cu_2O and Cu_2O/ZnO. Reproduced with permission from ref. 99 copyright 2021 Elsevier.

defect-rich $Bi_6Mo_2O_{15}$ sub-microwires with abundant oxygen vacancies, which could capture sufficient photo-generated electrons, are favorable for the photocatalytic reduction of CO_2 to CH_4.[93] Oxygen vacancies and metal vacancies can act synergistically to jointly improve the reaction selectivity.[102] Both oxygen and metal Ni vacancies were detected in NiCo-layered double hydroxide hollow nanocages (HC-NiCo-LDH), and the introduction of vacancies could create a new defect level in the middle of the band gap, causing a decreased band gap and enhanced charge transfer of HC-NiCo-LDH (Fig. 5c);[102] this guaranteed enough photo-induced electrons to reduce CO_2 molecules.[102] Finally, the CH_4 selectivity was increased from 8.92% to 62.66%.[102]

g-C_3N_4-based semiconductor composites could also selectively obtain CH_4 or other fuels.[112,113] Truc reported that compared with pure $Cu_2V_2O_7$ (*i.e.*, 0) and g-C_3N_4 (*i.e.*, 0), the $50Cu_2V_2O_7$/50g-C_3N_4 photocatalysts possessed more active electrons in the CB of the g-C_3N_4.[114] Enough electron supply of $50Cu_2V_2O_7$/50g-C_3N_4 accomplished the selective generation of CH_4 (*i.e.*, 1696 mmol g^{-1} cat. h^{-1}).[114] Additionally, in the g-C_3N_4/ZnO system, the electrons of ZnO recombined with the photo-generated holes of g-C_3N_4, thereby retaining the electrons with strong reduction capability in g-C_3N_4.[115] Sufficient electrons in the CB of g-C_3N_4 boosted the conversion of CO_2 to CH_3OH.[115] ZnO nanorod arrays@-carbon fiber (ZnO NA@CF) composites showed highly selective CH_3OH production during the photocatalytic CO_2 reduction.[116] Owing to the interaction between ZnO nanocrystals and carbon fiber, photo-generated electrons could transfer from ZnO to the surface of the carbon fiber, thus preventing the recombination of electron–hole pairs.[116] Photo-induced holes in the VB of ZnO reacted with water to produce O_2 and H^+, while CO_2 molecules were

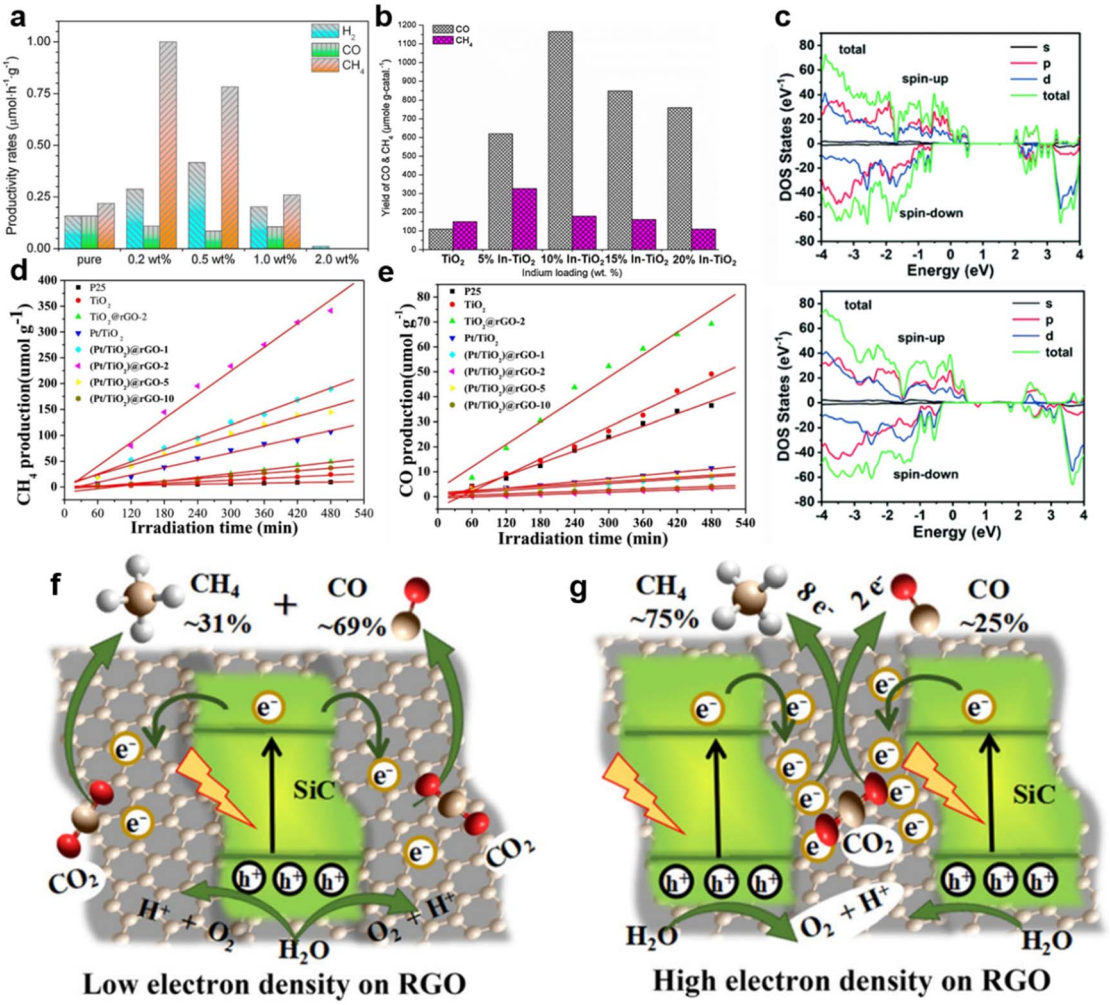

Fig. 5 (a) The production rates of pure TiO_2 and Mg–TiO_2 containing different amounts of Mg doping, reproduced with permission from ref. 100 copyright 2014 Elsevier. (b) The yield of products of In–TiO_2 with different amounts of In doping, reproduced with permission from ref. 101 copyright 2013 Elsevier. (c) Calculated total DOS (TDOS) and partial DOS (PDOS) plots of HC-NiCo-LDH without (upper) and with (lower) oxygen vacancies and Ni vacancies. Reproduced with permission from ref. 102 copyright 2018 Royal Society of Chemistry. (d) CH_4 production and (e) CO production over TiO_2, Pt/TiO_2, TiO_2@rGO-2 and (Pt/TiO_2)@rGO-*n* catalysts. Reproduced with permission from ref. 56 copyright 2018 Elsevier. A schematic illustration of the electron density-dependent CH_4 selective production over SiC/rGO heterojunctions with (f) low electron density and (g) high electron density on rGO. Reproduced with permission from ref. 103 copyright 2018 Wiley.

selectively reduced to CH_3OH by sufficient electrons on the carbon fiber.[116] rGO is another appealing photocatalyst that can accumulate electrons of high energy to accelerate CH_4 generation *via* an eight-electron catalytic process.[117] Bare rGO is not active for the photocatalytic conversion of CO_2 to CH_4 (ref. 56) but rGO-wrapped Pt/TiO_2 ((Pt/TiO_2)@rGO) photocatalysts achieved excellent selectivity (*i.e.*, 99.1%) of CH_4 evolution (Fig. 5d and e).[56] Pt nanoparticles in (Pt/TiO_2)@rGO-*n* photocatalysts functioned as an accumulator for electron transfer in the TiO_2–Pt–rGO ternary system.[56] Due to the strong electron-withdrawing capacity of the rGO shell, the photogenerated electrons could further transfer from Pt to rGO.[56] Thus, the photo-generated electrons were transferred from TiO_2 to Pt and finally to the rGO shell (*i.e.*, TiO_2 → Pt → rGO).[56] The photo-generated electrons accumulated on the rGO shell and subsequently reacted with the adsorbed CO_2 to produce CH_4.[56] The photo-excited electron transfer and accumulation process was also observed in SiC/rGO composites.[103] The electron density of the pure rGO surface was low.[103] In the SiC/rGO heterojunctions, the SiC served as the source of photogenerated electrons, while the rGO helped to quickly transfer energetic electrons for subsequent CO_2 reduction, resulting in a high CH_4 selectivity.[103] It is worth noting that by choosing a suitable ratio of SiC to RGO, a high electron density could be formed on the surface, thereby promoting the selective formation of CH_4 (Fig. 5f and g).[103] Additionally, crafting semiconductor composites might enhance photocatalytic selectivity *via* inducing oxygen vacancies.[109] Devi reported that the considerable carbon reduction selectivity of the In_2O_3–2wt% rGO nanocomposite (*i.e.* CH_4 generation rate of 953.72 μmol h^{-1} g^{-1} with the selectivity of ~74%) could mainly be attributed to the induced oxygen vacancy defects by the addition of rGO (Fig. 6a–c).[109]

The adjustment of the nanostructure and morphology of the materials can also change the accumulation of electrons, thereby facilitating the enhancement of photocatalytic performance in terms of selectivity. Pt-coated hexagonal boron nitride nanoreactors (Pt@h-BN) were synthesized by a two-step technique (Fig. 6d).[110] Among pure Pt, pure BN and the intermediate state BN before obtaining Pt-coated BN nanoreactors (Pt@IS-AB, middle part of Fig. 6d), Pt@h-BN with the Pt : B molar ratio of 1 : 3 (Pt@h-BN_3) demonstrated the best photocatalytic activity and achieved a nearly 100% selectivity of CO_2-to-CH_4 (Fig. 6e).[110] It was revealed that the special nanostructure composed of Pt as the core and h-BN as the shell (Fig. 6f and g)

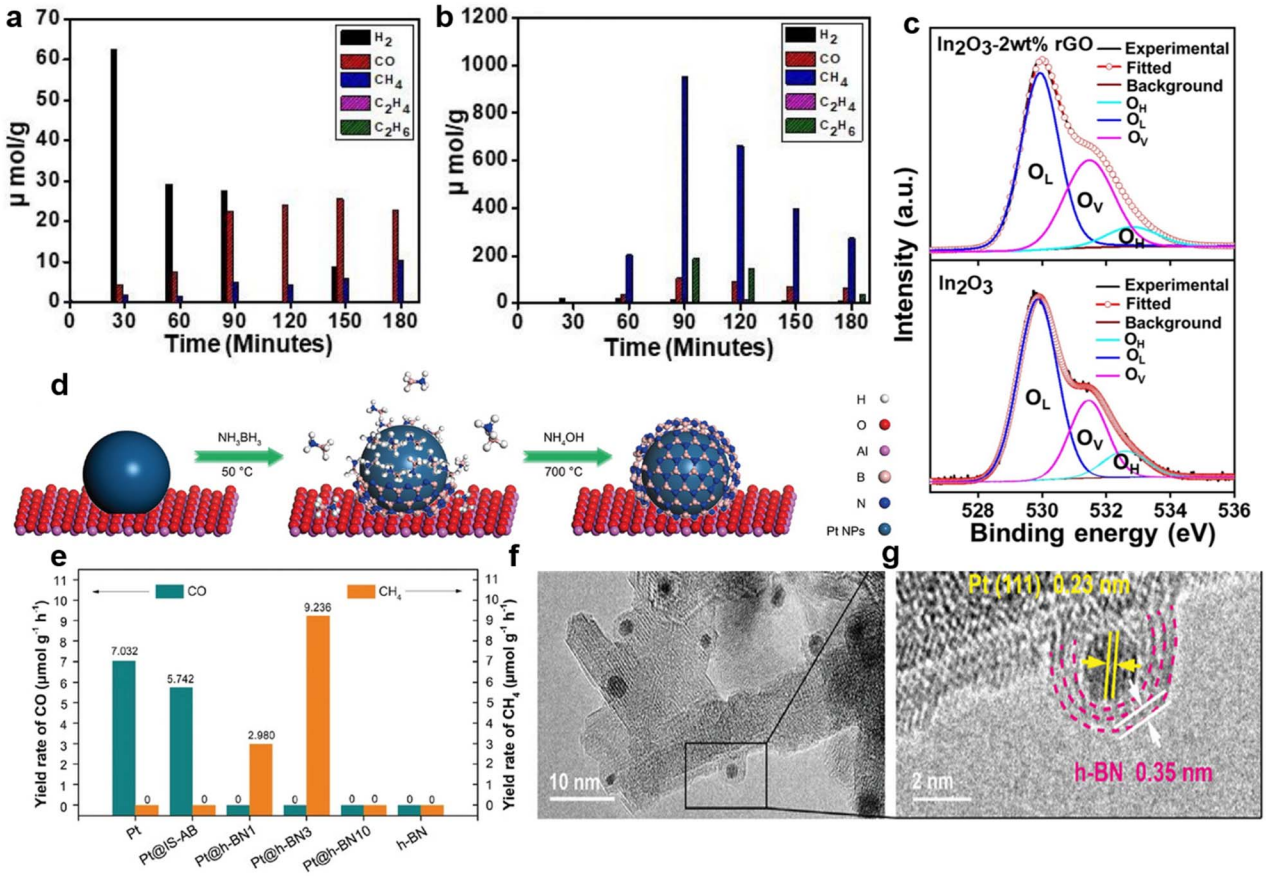

Fig. 6 Generation efficiency of various products over (a) In_2O_3 and (b) In_2O_3-2 wt% rGO. (c) High-resolution XPS spectra of O 1s of In_2O_3-2 wt% rGO nanocomposites (upper) and In_2O_3 nanostructures (lower). Reproduced with permission from ref. 109 copyright 2021 Elsevier. (d) Schematic diagram of the synthesis process of Pt@IS-AB and Pt@h-BN series catalysts originating from Pt. (e) The photocatalytic CO_2 conversion rate of Pt, Pt@IS-AB, Pt@h-BN series catalysts and pure h-BN. (f and g) HRTEM images of Pt@h-BN_3. Reproduced with permission from ref. 110 copyright 2021 Wiley.

accelerated the electron mobility to produce the key intermediate CO^{2-} species on the surface of Pt@h-BN.[110] Compared to pure $BiVO_4$, the lamellar $BiVO_4$ showed the selective generation of CH_3OH due to efficient electron capture to form $CO_2^{\bullet-}$ radical anions.[118] These provided researchers with a new method to construct highly selective photocatalysts by the delicate design of the architectures of photocatalysts.

Adequate electron supply is the most common mechanism to explain the selective reduction of CO_2 to CH_4 and other high-value-added products.

3.1.3. Others. As the active sites, metal ions, oxygen vacancies and metals loaded on the surface of photocatalysts are capable of the chemical conversion from CO_2 to specific products. Appropriate CO_2 adsorption together with efficient electron accumulation are proposed to cause high product selectivity.

For example, non-metals and metals can be co-doped into the lattice of the photocatalyst in order to accomplish high-efficiency selectivity.[119] The C and N co-doped TiO_2 nanotubes with Na^+ ions intercalated between the titanate layers were

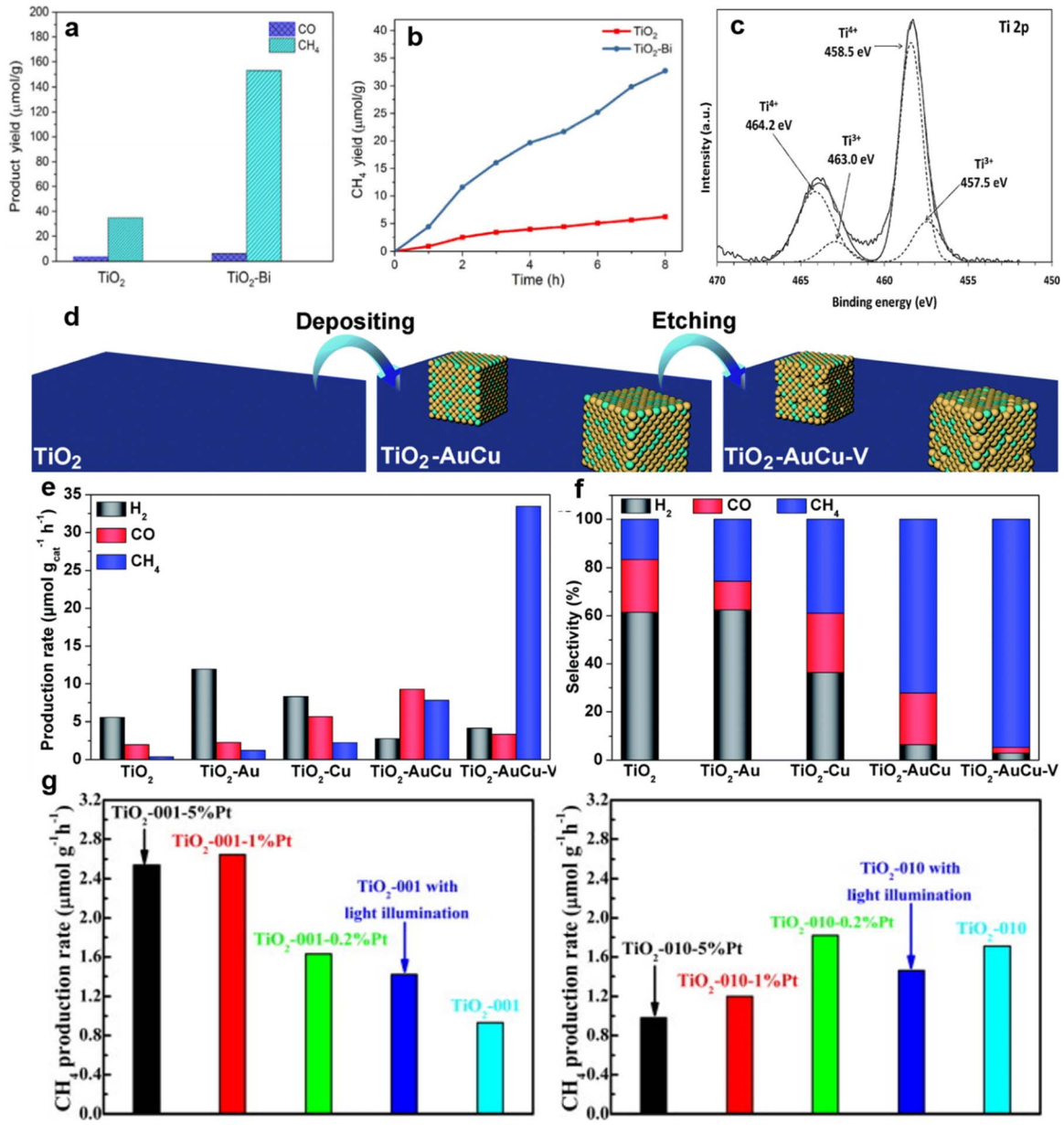

Fig. 7 (a) Product yields of TiO_2 and TiO_2–Bi after photocatalytic CO_2 reduction for 14 h. (b) Photocatalytic CH_4 generation of TiO_2 and TiO_2–Bi. Reproduced with permission from ref. 122. Copyright 2018 Springer. (c) A high-resolution XPS spectrum of Ti 2p of 10% I–TiO_2. Reproduced with permission from ref. 124. Copyright 2011 Elsevier. (d) The crafting process of TiO_2–AuCu–V. (e) Yields and (f) selectivity of CH_4, CO, H_2 over TiO_2-based photocatalysts. Reproduced with permission from ref. 125 copyright 2019 Royal Society of Chemistry. (g) Photocatalytic reduction activity of CO_2 to CH_4 over TiO_2-001 and TiO_2-010 and their corresponding 1 wt% or 5 wt% Pt-loaded products under UV-light irradiation for 4 h. Reproduced with permission from ref. 130 copyright 2014 Elsevier.

prepared by an alkaline hydrothermal method and achieved an increase in CH_4 yield.[120] Na^+ ions introduced on the surface of C–N co-doped TiO_2 nanotubes during the synthesis process were proposed to act as the active sites for effective CO_2 absorption and further increase the conversion of CO_2 to CH_4.[120] Similarly, compared with pure TiO_2, V and N co-doped TiO_2 nanocube arrays exhibited nearly four times improvement of photocatalytic CO_2 to CH_4 conversion.[121] In addition to the ions just mentioned, Bi^{3+} ions adsorbed on the surface of TiO_2 nanosheets favoured highly selective CH_4 photocatalytic production *via* stimulating the reduction of intermediate CO.[122] In this study, isolated Bi^{3+} ions were confined on the surface of 2D TiO_2 (TiO_2–Bi).[122] Compared with the pure TiO_2 counterpart, the TiO_2–Bi exhibited a higher photocatalytic selectivity and efficiency of CH_4 (Fig. 7a and b).[122] The mechanism was the consecutive transfer of protons and electrons to intermediate CO, finally producing CH_4, where the introduced Bi^{3+} was responsible for this fast conversion.[122] Furthermore, halogen element (*i.e.*, Cl, Br and I) doping can improve the catalytic selectivity.[123] XPS analysis of I-doped TiO_2 revealed that I^{5+} substituted for Ti^{4+} in the lattice (Fig. 7c).[124] As a result, Ti^{3+} was generated to balance the charge (Fig. 7c).[124] The high CO selectivity of I–TiO_2 was achieved after the I^{5+} doping.[124] We speculate that the low-valent titanium metal ions here are very likely to be used as active sites to promote the selective occurrence of the reaction, but direct experimental verification is needed.

Liu *et al.* loaded the Au–Cu alloy on TiO_2 nanosheets (TiO_2–AuCu) by ultrasonic and hydrothermal treatment and then obtained photocatalysts with Cu vacancies (TiO_2–AuCu–V) by etching (Fig. 7d).[125] In comparison with TiO_2, TiO_2–Au, TiO_2–Cu and TiO_2–AuCu, the CH_4 generation selectivity of TiO_2–AuCu–V was dramatically elevated to 94.7% (Fig. 7e and f).[125] The removal of Cu atoms at the surface of TiO_2–AuCu–V enhanced

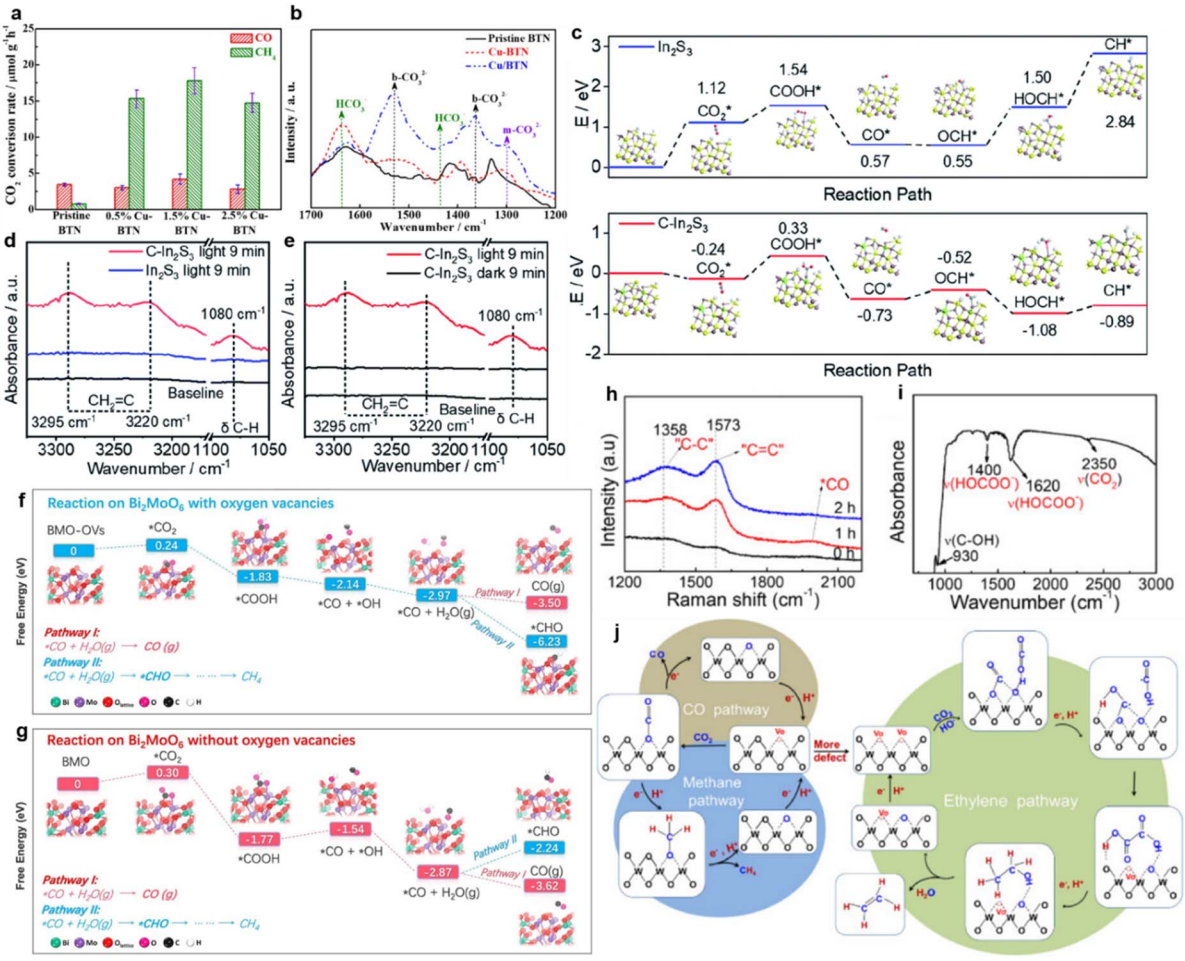

Fig. 8 (a) CO_2 photoreduction rate over pristine BTN and Cu-BTN with different amounts of Cu decoration. (b) *In situ* DRIFTS IR spectra of pristine BTN, Cu-BTN and Cu/BTN (obtained by depositing Cu on the as-prepared brookite TiO_2 nanocubes). Reproduced with permission from ref. 61 copyright 2017 Wiley. (c) Calculated reaction energy diagrams of CO_2 to CH* over the H-terminated surfaces of pristine In_2S_3 and C–In_2S_3. *In situ* DRIFTS spectra of (d) In_2S_3 and (e) C–In_2S_3. Reproduced with permission from ref. 133 copyright 2020 Royal Society of Chemistry. Reaction pathways of CO_2 reduction over $BiMoO_6$ (f) with oxygen vacancies and (g) without oxygen vacancies. Reproduced with permission from ref. 63 copyright 2019 Elsevier. (h) Raman spectra of WO_{3-x} during the photocatalytic CO_2 reduction. (i) IR spectrum of WO_{3-x} after photocatalysis. (j) Schematic diagram of possible pathways of C_2H_4, CH_4 and CO generation *via* photocatalytic CO_2 reduction over WO_{3-x}. Reproduced with permission from ref. 62 copyright 2020 Elsevier.

the electron trapping ability, consequently providing sufficient electrons for the generation of CH_4 as mentioned above.[125] Moreover, the experimental results also showed that there is a strong correlation between the yield of CH_4 and the low-coordination Cu atoms near the vacancies, indicating that these Cu atoms could be used as active sites for the conversion of CO_2 to CH_4, further enhancing the selectivity of CH_4 generation.[125]

Interestingly, although some metals have been proven to be able to improve selectivity in research, the same kind of metal loaded on different crystal faces of a special catalyst may exhibit different site activities. Taking the commonly used anatase TiO_2 catalyst as an example, the theoretical surface energy order of the low index facets is {101} (*i.e.*, 0.44 J m^{-2}) < {010} (*i.e.*, 0.53 J m^{-2}) < {001} (*i.e.*, 0.90 J m^{-2}).[126,127] This means that the most stable {101} facets exhibit the lowest catalytic reactivity for the CO_2 reduction. Thus, in order to manipulate products and achieve high photocatalytic efficiency, ratios of {001} to {010} TiO_2 exposed facets were tuned.[128] Due to the strong interaction between CO_2 and the {010} surface of TiO_2, anatase TiO_2 rods with dominant {010} facets accomplished the efficient photoreduction of CO_2 to CH_4.[128] Ma reported that after Pt loading, anatase TiO_2 exposing {001} facets exhibited improved CH_4 evolution rates.[129] After modifying Pt on {001}TiO_2 facets, uniform Pt nanoparticles acted as active sites and led to a higher CH_4 yield.[130] However, when decorated on the {010} TiO_2 facets, Pt nanoparticles agglomerated, exerting a negative effect on the photocatalytic reaction (Fig. 7g).[130]

To sum up, the introduction of metals, vacancies, and different ions to the photocatalysts might serve as active sites for the selective conversion of CO_2 to the target products. However, the relationship between the active sites and the high reaction selectivity is not clear. The roles of some special ions, such as low-valence metal ions (Ti^{3+}) generated together with the Vo (Fig. 7c) during the selective CO_2 reduction reaction have not been fully assessed. Many of the discussions about the active sites just put forward conjectures that need to be further investigated by experiment.

3.2. Intermediates

3.2.1. Formation energy of crucial intermediates. To produce high-value-added products, the formation of some key intermediates is particularly significant.[131,132] Taking the selective formation of CH_4 as an example. There are two reaction paths after the formation of *CO. One is that *CO is released from the surface to generate CO, and the other is that *CO is hydrogenated to generate *CHO and finally converted to CH_4. It can be seen that the formation energy of *CHO is lower than that of *CO, and the reaction is inclined to generate CH_4. The formation energy of intermediates could be reduced *via* metal loading, vacancy construction and ion modification.

Cu-nanocluster-decorated brookite TiO_2 quasi-nanocubes (Cu-BTN) exhibited good activity and selectivity (Fig. 8a).[61] When using 1.5% Cu-BTN as photocatalysts, the main products were CH_4, accounting for about 85% of the total amount of final products.[61] The reason for this high photocatalytic selectivity of Cu-BTN was explained as follows. When CO_3^{2-} ions were intermediates, CO would be the main product, while more CH_4 would be produced if HCO_3^- ions were intermediates.[61] With the introduction of Cu nanoclusters and the gradual increase within the appropriate range, the formation of HCO_3^- on the surface of Cu-BTN would become easier (Fig. 8b); finally, CH_4 would be formed selectively.[61]

In addition to the experimental characterization of the formation of key intermediates, the free energy of intermediate formation was studied through theoretical calculations. Wang achieved a C_2H_4 production selectivity close to 50% over C-doped In_2S_3 nanosheets.[133] According to the calculated reaction energy, the reaction Gibbs free energies from OCH* to HOCH* and from HOCH* to CH* on C–In_2S_3 were −0.56 and 0.19 eV, respectively, which were much lower than the corresponding energies on pure In_2S_3 (*i.e.*, 0.95 and 1.34 eV), respectively (Fig. 8c).[133] It was indicated that OCH* could be further hydrogenated to form CH* on C–In_2S_3 (Fig. 8d and e).[133] Meanwhile, unsaturated *CH_2=C, one of the important intermediates to produce C_2H_4, could be observed on the surface of C–In_2S_3 in the *in situ* DRIFTS spectra, which was not detected on pure In_2S_3 (Fig. 8d and e).[133]

Similarly, Yang *et al.* prepared Bi_2MoO_6 nanosheets containing oxygen vacancies *via* a facile one-step solvothermal process.[63] According to the calculated stepwise Gibbs free energy (Fig. 8f and g), the further hydrogenation of the intermediate CO* to the *CHO over Bi_2MoO_6 with oxygen vacancies was thermodynamically supported, compared to Bi_2MoO_6 without oxygen vacancies.[63] Since *CHO was the prerequisite for the synthesis of CH_4, it could be accompanied by the subsequent hydrogenation steps, ultimately realizing the highly selective CH_4 production of 96.7% under visible light irradiation.[63] The tuning of the energy barrier by oxygen vacancies was further confirmed on the surface of Ni–TiO_2.[136] Besides the theoretical calculations, the important intermediate formation could be identified by experiments.[62] For instance, the photocatalytic selectivity of WO_{3-x} micro-rods reducing CO_2 to C_2H_4 increased to 89.3% after introducing oxygen vacancies.[62] It could be observed in Raman and Infrared (IR) spectra that essential intermediates, including C=C, C–C, adsorbed CO and HOCOO, appeared (Fig. 8h and i). It was indicated that adjacent oxygen vacancies provided active sites for C–C coupling to generate C_2H_4. The CO_2 reduction pathway on the WO_{3-x} was proposed to be CO_2 → ·COOH → $(COOH)_2$ → CH_3COOH → CH_3CH_2OH → CH_2CH_2 *via* a hydrogenation and dehydration process (Fig. 8j).[62] Apart from the reactions mentioned above, CO_2 could also be selectively reduced to methanol, formic acid and other hydrocarbons.[74,75,137] For example, the energy barrier of the rate-limiting step (CO_2 → HCOO) on the surface of MXene (0.53 eV) for the reduction of CO_2 to HCOOH is much lower than that of anatase (0.87 eV), which was prone to producing HCCOH.[97]

Besides, metal vacancies of semiconductors can adjust the formation energy of intermediates, thereby affecting the photocatalytic reaction.[134] Since ZnS samples possessing Zn vacancies could be obtained by acid etching over commercial ZnS powders, different pH values of sulfuric acid were used to craft

ZnS containing various amounts of Zn vacancies and obtained different HCOOH formation selectivities (Fig. 9a and b).[134] Acid-etched ZnS attained the highest selectivity of 86.6% for HCOOH production at pH = 0.2.[134] As displayed in Fig. 9c, with the existence of Zn vacancies, ZnS required a lower energy barrier for the reduction of CO_2 to HCOOH.[134] Moreover, hydroxyl groups on the surface might bind closely with CO_2 molecules to form key intermediates during the photocatalytic CO_2 reduction.[135] The proposed CH_4 formation mechanism on the hydroxylated mesoporous TiO_2 surface is shown in Fig. 10d.[135] According to the experimental results, on the hydroxyl-abundant surface of TiO_2, the –OH groups could convert absorbed CO_2 molecules to carbonate or bicarbonate species (Fig. 9d).[135] The bidentate carbonate (b-CO_3^{2-}) species sequentially received 2 electrons and 2 protons and were transformed into CH_4 through the sequence of Ti–$OOCH_2$ → Ti–O–CH_3 →

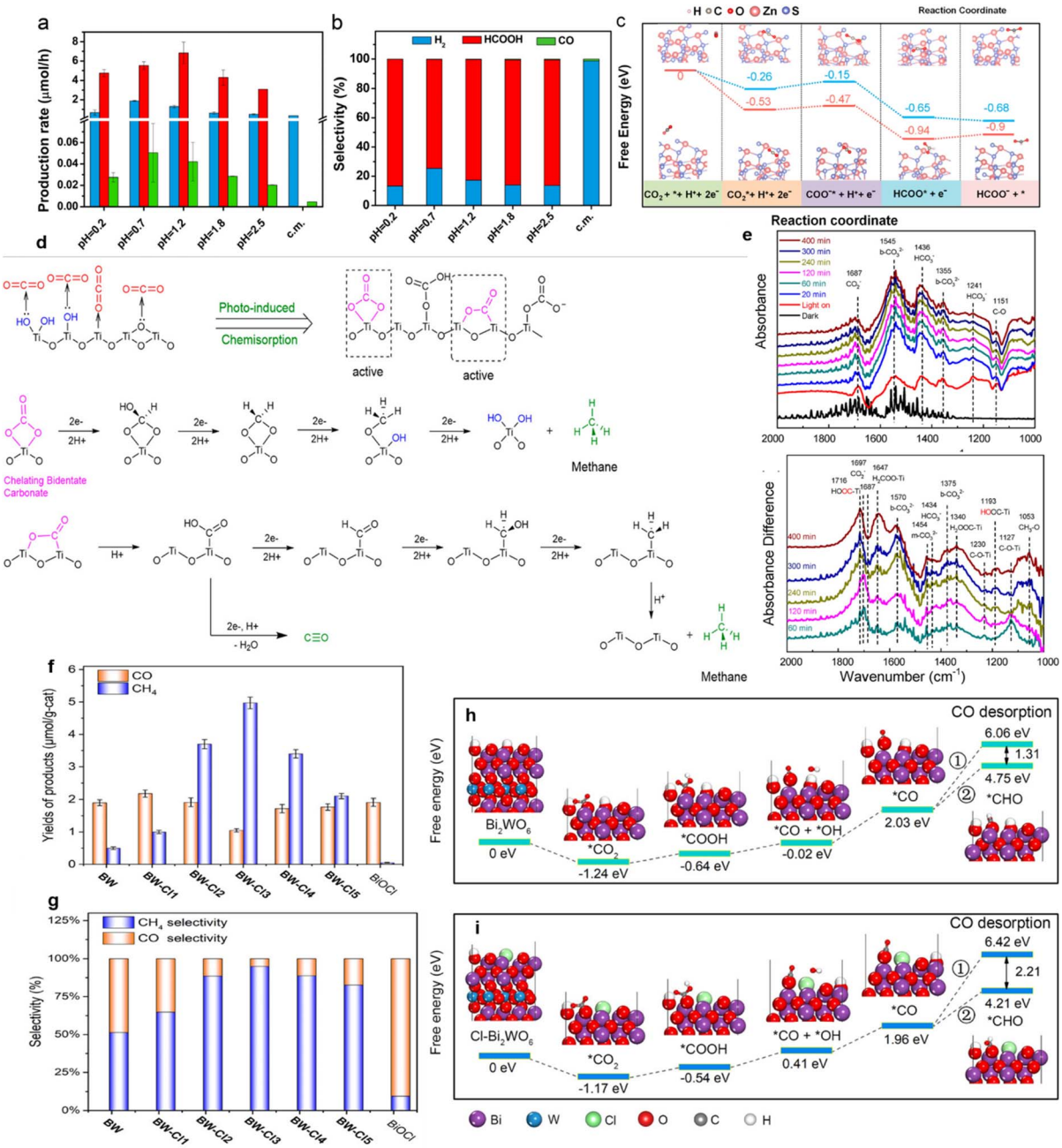

Fig. 9 (a) Yields and (b) selectivity of HCOOH, CO, H_2 over ZnS samples etched by sulfuric acid of different pH values. (c) Free energy diagram for the pathways of CO_2 conversion to formate on a perfect ZnS (blue) and V_{Zn}-ZnS (pink) surface. Reproduced with permission from ref. 134 copyright 2019 American Chemical Society. (d) Proposed CH_4 and CO formation mechanism on the hydroxylated surface of TiO_2. (e) The DRIFT spectra of adsorbed and transformed species on the hydroxylated surface of TiO_2 after different light irradiation times. Reproduced with permission from ref. 135 copyright 2020 American Chemical Society. (f) Yields and (g) selectivity of CO and CH_4 over BW, BiOCl, and BW–Cl_x (x = 1–5) after photocatalytic CO_2 reduction for 3 h. Free energy diagrams of CO_2 photoreduction over (h) Bi_2WO_6 and (i) Cl^--modified Bi_2WO_6. Reproduced with permission from ref. 70 copyright 2020 American Chemical Society.

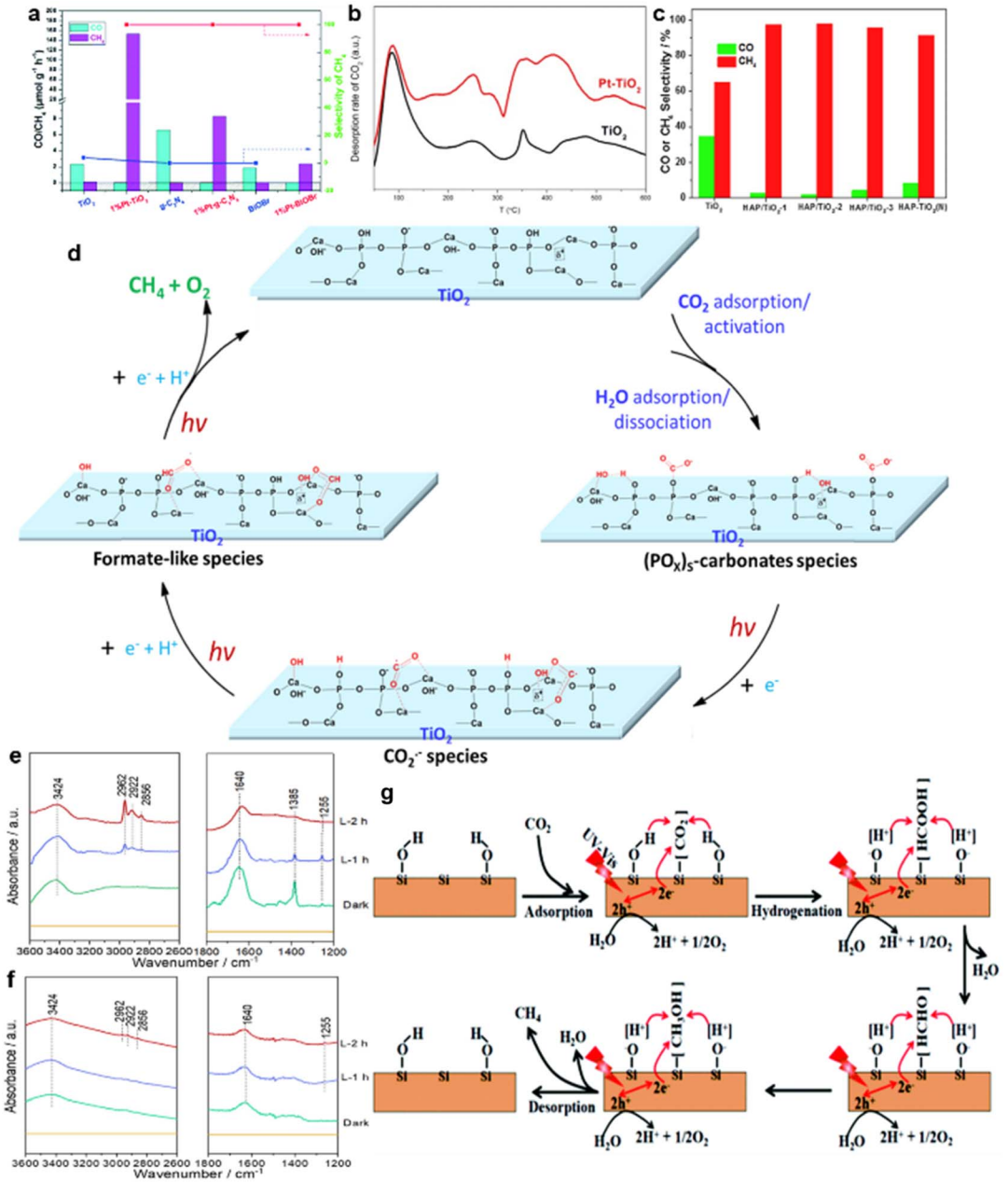

Fig. 10 (a) Photocatalytic activities and selectivities of CO_2 reduction over TiO_2, g-C_3N_4 and BiOBr with or without Pt loading. (b) CO-TPD of TiO_2 and Pt–TiO_2. Reproduced with permission from ref. 58 copyright 2018 Royal Society of Chemistry. (c) The evolution rates and the selectivity of CO and CH_4 over TiO_2 and various HAP/TiO_2 photocatalysts. (d) A possible pathway for the conversion of CO_2 to CH_4 over Pt/HAP/TiO_2 in the presence of H_2O. *In situ* IR spectra of (e) Pt/HAP/TiO_2 and (f) Pt/TiO_2.[68] Reproduced with permission from ref. 68 copyright 2018 Elsevier. (g) Schematic illustration of the photocatalytic CO_2 conversion to CH_4 over hydroxylated SiC nanosheets. Reproduced with permission from ref. 141 copyright 2019 Royal Society of Chemistry.

CH_4 (Fig. 9d).[135] Meanwhile, the carboxylic species experienced the process of Ti–COOH → Ti–CHO → Ti–CH_2OH → Ti–CH_3 → CH_4 to produce CH_4 (Fig. 9e).[135]

Ion modification can also improve the selectivity of CO_2 reduction by adjusting the formation energy of key intermediates.[138] Li prepared Bi_2WO_6 (BW) nanosheets loaded with different amounts of Cl^- ions, which were marked as BW–Cl_x (x = 1–5).[70] A maximum selectivity of 94.98% for CH_4 generation was achieved on the surface of BW–Cl_3 (Fig. 9f and g).[70] In the presence of Cl^- ions, the half-reaction (*i.e.*, oxygen evolution) of Bi_2WO_6 nanosheets was greatly increased.[70] Simultaneously, the produced protons facilitated the formation of CH_4.[70] Moreover, DFT calculations (Fig. 9h and i) confirmed that the presence of Cl^- ions on Bi_2WO_6 nanosheets was capable of lowering the energy barrier for the generation of crucial intermediate (*i.e.*, *CHO), thus enhancing CH_4 production.[70]

In the above reports, the existence of key intermediates in some highly selective systems was verified by the experimental

data, and the formation energy of the target intermediates was studied through theoretical calculations. The difficulty in producing intermediates and the stability of the as-obtained intermediates will be discussed in the next section.

3.2.2. Stability of intermediates. In order to synthesize high-value-added products, the stability of target intermediates should be taken into account.[139] Stable intermediates facilitate electron transfer reactions in the subsequent hydrogenation process, while instability would lead to rapid desorption from the surface of photocatalysts and the reaction ends at this step. As mentioned in the previous section, the intermediate *CHO is crucial for the formation of CH_4, and it should be guaranteed that not only the formation energy of *CHO is low, but also *CHO is stable enough to generate CH_4. The high stability of key intermediates could be achieved through the loading of precious metals and the combination of different materials.

For instance, the introduction of noble metals could reduce the intermediate desorption capacity of the photocatalysts and ensure that the intermediates are adsorbed on the surface of the catalysts for subsequent reactions.[58] As shown in Fig. 10a, compared with pure semiconductor photocatalysts, nearly 100% selectivity of CH_4 generation was achieved by loading 1% Pt on the TiO_2, C_3N_4 and BiOBr photocatalysts, respectively.[56,58,140] The temperature-programmed desorption (TPD) results confirmed that CO demonstrated an especially strong adsorption capacity on the Pt clusters (Fig. 10b).[58] Meanwhile, since only physical adsorption occurred between CH_4 and the Pt clusters, CH_4 exhibited low adsorption energy on the Pt clusters, leading to the easy desorption of generated CH_4 from the Pt surface.[58] Thus, most CO products produced during the photocatalytic process were anchored on the catalyst surfaces, and CH_4 molecules were desorbed from the photocatalyst surface, eventually achieving enhanced selectivity of CH_4 generation.[58]

Through compound modification of the catalysts, the stability of some key intermediates can also be improved. Hydroxyapatite (HAP)-decorated TiO_2 could achieve 99.1% selectivity of CH_4 generation (Fig. 10c).[68] The formation of much more stable intermediates over HAP/TiO_2 nanorods was responsible for this selectivity enhancement.[68] A possible pathway for the conversion of CO_2 to CH_4 over Pt/HAP/TiO_2 in the presence of H_2O is proposed in Fig. 10d.[68] Specifically, the formate-like species ($HCOO^-$) was identified as the crucial intermediate for CH_4 production.[68] Compared with that of TiO_2, IR peaks at 3000–2800 cm^{-1} of Pt/HAP/TiO_2 were obviously enhanced, indicating that the HAP effectively improved the stability of $HCOO^-$ (Fig. 10e and f).[68]

Besides, as the cocatalyst of P25, surface alkalization of Ti_3C_2 could dramatically enhance the evolution rate of CH_4 (16.61 μmol g^{-1} h^{-1}),[142] in which surface hydroxyls on selective CH_4 generation over SiC nanosheets have gained much attention.[141,143] Hydroxyl groups on the surface of SiC nanosheets boosted the photoreduction of CO_2 into CH_4, achieving the CH_4 generation selectivity of about 80%.[141] The mechanism is depicted in Fig. 10g.[141] Specifically, –OH groups on the surface of SiC could provide sufficient protons to CO_2, which is critical to the CO_2 activation.[141] Moreover, the intermediates could be stabilized by forming hydrogen bonds between the intermediates and –OH groups. These effects improved the selective CH_4 generation.[141]

Although the stability of the intermediates remarkably affects the reaction path of photocatalytic CO_2 reduction, the relative investigations are limited in scope. More attention should be paid to the generation process and stabilization of key intermediates to make the study on CO_2 reduction more comprehensive and convincing.

3.3. Desorption of products

As one critical step in the entire CO_2 reduction process, the desorption of the product from the surface of photocatalysts affects the selectivity. The rapid release of the product prevents the subsequent reaction, thereby maintaining the selective and continuous yield of this product. Various types of vacancies and crystal facets cause varied adsorption capabilities of products, which results in the adjustment of the final products.

Metal vacancies of semiconductors play a significant role in manipulating the photocatalytic selectivity. Different reduction products can be obtained by introducing various metal vacancies.[144] Selective CO generation could be achieved on the surface of BiOBr ultrathin nanosheets containing abundant Bi vacancies (V_{Bi}).[144] Compared with BiOBr nanosheets without V_{Bi}, CO could be more easily desorbed from the surface of V_{Bi}–BiOBr, leading to increasing the amount of CO production.[144]

In addition to the introduction of vacancies, some facets of photocatalysts may exhibit the unique ability of CO_2 adsorption and product desorption.[145–147] These beneficial effects can enhance the photocatalytic selectivity. As shown in Fig. 11a, distinguished from chemisorbed CO with a larger endothermic

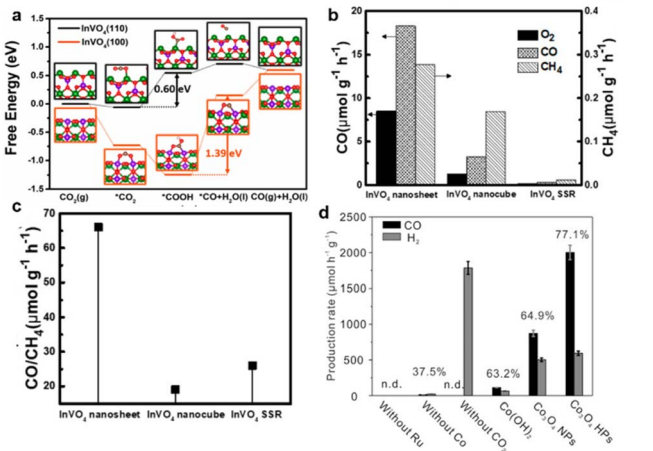

Fig. 11 (a) The photocatalytic activity and (b) the production rates of CO to CH_4 over the ultrathin $InVO_4$ nanosheets, nanocubes, and obtained by SSR. (c) Calculated Gibbs free energy profiles of photocatalytic CO_2 reduction to CO over $InVO_4$ of the (110) and (100) planes, respectively. Reproduced with permission from ref. 148 copyright 2019 American Chemical Society. (d) Photocatalytic production rate using β-$Co(OH)_2$, Co_3O_4 nanoparticles (Co_3O_4 NPs), or Co_3O_4 hexagonal platelets (Co_3O_4 HPs) as catalysts under visible light ($\lambda > 420$ nm) irradiation. Reproduced with permission from ref. 150 copyright 2016 Wiley.

value of 0.45 eV on the {100} facet, the exposed {110} facet of the $InVO_4$ atomic layer was confirmed to weakly bind the generated CO, leading to the quick desorption of CO molecules from the catalyst surface.[148] Therefore, by the facet engineering technique, ultrathin $InVO_4$ nanosheets possessing the {110} facet could gain much higher CO formation selectivity (*i.e.*, 98%) as compared with regular $InVO_4$ nanocubes showing the (100) facet and the bulk $InVO_4$ obtained by a conventional solid-state reaction (SSR, Fig. 11b and c).[148] Due to the favorable CO_2 absorption and easy desorption of CO, hexagonal Co_3O_4 nanoplatelets exposing {112} facets could realize the selectivity of 77.1% for CO generation (Fig. 11d).[149]

In general, both metal vacancies and crystal facets have selective desorption capacity. However, it is unknown whether other modification methods could mediate the desorption ability of products. There is limited discussion in this area, and further exploration is expected.

4. Summary and outlook

There has been widespread interest in the fact that photocatalytic product selectivity is one of the crucial factors limiting the application of photocatalytic CO_2 reduction. The importance of photocatalytic CO_2 reduction to energy utilization and environmental protection is summarized at the beginning of this review. We introduced different reaction steps that could increase the selectivity of the reaction, that is, the adsorption and activation of reactants (including CO_2 adsorption and H_2 evolution inhibition, electron supply and others), the formation and stabilization of intermediates (including formation energy of crucial intermediates and stability of intermediates), and the desorption of products. The corresponding modification methods for achieving selective improvement at each stage are summarized, including noble metal decoration, metal and nonmetal doping, vacancy engineering, facet engineering, composite construction, hydroxyl modification and other decoration techniques. Although this research field has been developed for several decades, the photocatalytic conversion of CO_2 to high-value products selectively is still in its infancy. A lot of effort should be made to achieve a great breakthrough.

Firstly, although many materials have been successfully fabricated for highly selective photocatalytic CO_2 reduction, the photocatalytic mechanism of high selectivity remains unclear. Most mechanisms have been proposed based on the simulation results instead of experimental data. In addition, plenty of intriguing phenomena, such as the formation of low-valent metal ions near the oxygen vacancies, and the production of surface hydroxyl groups, have been described but no explanations are given in detail. Therefore, more *in situ* characterization techniques, such as FITR, Raman, XRD and NMR, should be conducted to uncover the underlying photocatalytic process. To design highly selective catalysts on purpose, a deep understanding and exploration of the reaction must be gained.

Secondly, more investigations should be focused on the oxidation reaction during photocatalytic CO_2 reduction. Since main products are obtained *via* reducing CO_2, most research is concentrated on the reduction reaction caused by the photogenerated electrons. However, as a half-reaction of the entire CO_2 reduction, how photo-induced holes participate in the photocatalytic reaction might dramatically affect the catalytic performance of semiconductors. Once the oxidation reaction is restricted, it will be tough for the entire process to proceed. A quick oxidation half-reaction can suppress the inverse reactions of CO_2 reduction. In addition, the oxidation products might participate in the reaction of CO_2 reduction. Therefore, to have a comprehensive understanding of the entire CO_2 reduction process, the oxidation half-reaction involving photo-generated holes requires more in-depth investigations.

Thirdly, precise modification techniques of photocatalysts should be further improved. The introduction of impurities into the lattice of semiconductors can increase the effective capture of electrons and thus improve the selectivity of CH_4 generation. However, there is always an optimal doping concentration. Similarly, the construction of vacancies can bring about an increase in selectivity but excessive vacancies will destroy the bulk structure and reduce the catalytic performance. More delicate methods should be developed to craft decorated photocatalysts.

Fourthly, based on this review, it was found that each step during the entire CO_2 reduction can affect selectivity, so different modification methods could be combined to synergistically boost the reaction selectivity. For example, after oxygen vacancies were introduced into Pt-loaded Ga_2O_3, the selectivity of the reaction increased to nearly 100%.[81] The oxygen vacancies served as the main sites for CO_2 adsorption, while Pt nanoparticles used the hydrogen formed in the photocatalytic decomposition process to reduce the adsorbed CO_2.[81] This synergy increased photocatalytic production selectivity.[81] Besides, the photocatalytic conditions of the catalytic system can influence the production selectivity, including temperature, pressure, gas flow rate, reaction solution, *etc.* Thus, more explorations can be concentrated on adjusting the composition of photocatalysts and the reaction parameters.

In summary, photocatalytic CO_2 conversion to fuel products can not only alleviate carbon dioxide emissions but also provide clean chemical energy using green solar light. To realize high catalytic efficiency and achieve value-added products of high selectivity, the above four points require numerous efforts to explore. More advanced *in situ* characterization techniques, including solid-state NMR, isotope research, FITR, Raman, and XRD should be applied to study the chemical evolution of catalysts during the catalytic process. To understand the entire reaction process more comprehensively, more studies should be conducted that pay attention to both the reduction half-reaction and the oxidation half-reaction since how photo-induced electrons and holes participate in the photocatalytic reaction will affect the catalytic performance. Due to the different effects of various modification strategies on the reaction process, the modification process should be controlled more accurately, which requires more advanced synthesis equipment and more delicate fabrication strategies. Different modification techniques could be combined to synergistically achieve higher efficiency and selectivity.

Author contributions

M. W. conceived the idea. M. W., S. Y. designed the conceptualization. S. Y., J. H., F. G., H. W., J. L., Y. B. performed the investigation and data curation. J. F., F. H., F. Z. conducted the supervision. M. W., S. Y. wrote the paper. All authors participated in the review and editing of the paper.

Conflicts of interest

There are no conflicts to declare.

Acknowledgements

Mengye Wang gratefully acknowledges the financial support from the National Natural Science Foundation of China (No. 21905317), the Young Elite Scientists Sponsorship Program by CAST (2019QNRC001), and the Fundamental Research Funds for the Central Universities, Sun Yat-sen University (76180-31620007).

Notes and references

1 I. L. T. M. S. Dresselhaus, *Nature*, 2001, **414**, 332–337.
2 F. Liu, M. Wang, X. Liu, B. Wang, C. Li, C. Liu, Z. Lin and F. Huang, *Nano Lett.*, 2021, **21**, 1643–1650.
3 Q. Liu, X. Hong, X. You, X. Zhang, X. Zhao, X. Chen, M. Ye and X. Liu, *Energy Storage Mater.*, 2020, **24**, 541–549.
4 S. Yao, J. Liu, F. Liu, B. Wang, Y. Ding, L. Li, C. Liu, F. Huang, J. Fang, Z. Lin and M. Wang, *Environ. Sci. Nano*, 2022, **9**, 1996–2005.
5 S. Han, Q. Wan, K. Zhou, A. Yan, Z. Lin, B. Shu and C. Liu, *ACS Appl. Nano Mater.*, 2021, **4**, 8273–8281.
6 Y. Li, L. Li, F. Liu, B. Wang, F. Gao, C. Liu, J. Fang, F. Huang, Z. Lin and M. Wang, *Nano Res.*, 2022, **15**, 7986–7993.
7 J. He, F. Gao, H. Wang, F. Liu, J. Lin, B. Wang, C. Liu, F. Huang, Z. Lin and M. Wang, *Environ. Sci. Nano*, 2022, **9**, 1952–1960.
8 Z. Wang, J. Zheng, M. Li, Q. Wu, B. Huang, C. Chen, J. Wu and C. Liu, *Appl. Phys. Lett.*, 2018, **113**, 122101.
9 Y. Wang, Z. Wang, K. Huang, X. Liang, C. Liu, C. Chen and C. Liu, *Appl. Phys. Lett.*, 2020, **116**, 141604.
10 X. Liang, L. Liu, G. Cai, P. Yang, Y. Pei and C. Liu, *J. Phys. Chem. Lett.*, 2020, **11**, 2765–2771.
11 D. Moreira and J. C. M. Pires, *Bioresour. Technol.*, 2016, **215**, 371–379.
12 F. Barzagli, C. Giorgi, F. Mani and M. Peruzzini, *J. CO_2 Util.*, 2017, **22**, 346–354.
13 W. P. Wang Zeyan, Y. Liu, Z. Zheng, H. Cheng and B. Huang, *J. Synth. Cryst.*, 2021, **50**, 685–707.
14 S. Chu and A. Majumdar, *Nature*, 2012, **488**, 294–303.
15 M. Wang, B. Wang, F. Huang and Z. Lin, *Angew. Chem., Int. Ed. Engl.*, 2019, **58**, 7526–7536.
16 X. Zhang, F. Xie, X. Li, H. Chen, Y. She, C. Wang, Z. Mo, W. Yang, P. Hou, C. Wu, H. Xu and H. Li, *Appl. Surf. Sci.*, 2021, **542**, 148619.
17 Y. Wang, S. Z. F. Phua, G. Dong, X. Liu, B. He, Q. Zhai, Y. Li, C. Zheng, H. Quan, Z. Li and Y. Zhao, *Chem*, 2019, **5**, 2775–2813.
18 C. W. W. Ng, R. Tasnim and J. L. Coo, *Eng. Geol.*, 2018, **242**, 108–120.
19 D. R. Feldman, W. D. Collins, P. J. Gero, M. S. Torn, E. J. Mlawer and T. R. Shippert, *Nature*, 2015, **519**, 339–343.
20 J. Cai, J. Shen, X. Zhang, Y. H. Ng, J. Huang, W. Guo, C. Lin and Y. Lai, *Small Methods*, 2019, **3**, 1800184.
21 J. Xiong, J. Luo, J. Di, X. Li, Y. Chao, M. Zhang, W. Zhu and H. Li, *Fuel*, 2020, **261**, 116448.
22 J. Bonin, A. Maurin and M. Robert, *Coord. Chem. Rev.*, 2017, **334**, 184–198.
23 M. Wang, L. Cai, Y. Wang, F. Zhou, K. Xu, X. Tao and Y. Chai, *J. Am. Chem. Soc.*, 2017, **139**, 4144–4151.
24 M. Wang, Y. Zuo, J. Wang, Y. Wang, X. Shen, B. Qiu, L. Cai, F. Zhou, S. P. Lau and Y. Chai, *Adv. Energy Mater.*, 2019, **9**, 1901801.
25 Q. Wang, J. Cai, G. V. Biesold-McGee, J. Huang, Y. H. Ng, H. Sun, J. Wang, Y. Lai and Z. Lin, *Nano Energy*, 2020, **78**, 105313.
26 F. He, X. You, H. Gong, Y. Yang, T. Bai, W. Wang, W. Guo, X. Liu and M. Ye, *ACS Appl. Mater. Interfaces*, 2020, **12**, 6442–6450.
27 C. He, B. Han, S. Han, Q. Xu, Z. Liang, J. Y. Xu, M. Ye, X. Liu and J. Xu, *J. Mater. Chem. A*, 2019, **7**, 26884–26892.
28 G. Feng, H. Jiaqing, W. Haowei, L. Jiahui, C. Ruixin, Y. Kai, H. Feng, L. Zhang and W. Mengye, *Nano Res. Energy*, 2022, **1**, e9120029.
29 E. V. Kondratenko, G. Mul, J. Baltrusaitis, G. O. Larrazábal and J. Pérez-Ramírez, *Energy Environ. Sci.*, 2013, **6**, 3112–3135.
30 Y. Chen, G. Jia, Y. Hu, G. Fan, Y. H. Tsang, Z. Li and Z. Zou, *Sustain. Energy Fuels*, 2017, **1**, 1875–1898.
31 S. Zhu, Q. Wang, X. Qin, M. Gu, R. Tao, B. P. Lee, L. Zhang, Y. Yao, T. Li and M. Shao, *Adv. Energy Mater.*, 2018, **8**, 1802238.
32 K. Hua, X. Liu, B. Wei, S. Zhang, H. Wang and Y. Sun, *Acta Phys.-Chim. Sin.*, 2020, 2009098.
33 P. Zhou, J. Yu and M. Jaroniec, *Adv. Mater.*, 2014, **26**, 4920–4935.
34 G. Xiaoya, L. Jiaofu and Z. Zicheng, *Nano Research Energy*, 2022, **1**, e9120036.
35 X. O. Bin Han, Z. Zhong, S. Liang, Y. Xu, H. Deng and Z. Lin, *Appl. Catal., B*, 2021, 283119594.
36 J.-N. Zhang, N. K. Niazi, J. Qiao, L. Li, I. M. u. Hasan, R. He, L. Peng, N. Xu and F. Farwa, *Nano Research Energy*, 2022, **1**, e9120015.
37 X. Xiong, Y. Zhao, R. Shi, W. Yin, Y. Zhao, G. I. N. Waterhouse and T. Zhang, *Sci. Bull.*, 2020, **65**, 987–994.
38 J. Z. Han Li, J. Yu and S. Cao, *Trans. Tianjin Univ.*, 2021, **27**, 338–347.
39 A. Corma and H. Garcia, *J. Catal.*, 2013, **308**, 168–175.
40 D. D. Zhu, J. L. Liu and S. Z. Qiao, *Adv. Mater.*, 2016, **28**, 3423–3452.

41 C. W. Kim, M. J. Kang, S. Ji and Y. S. Kang, *ACS Catal.*, 2018, **8**, 968–974.
42 Z. Wu, S. Guo, L.-H. Kong, A.-F. Geng, Y.-J. Wang, P. Wang, S. Yao, K.-K. Chen and Z.-M. Zhang, *Chinese J. Catal.*, 2021, **42**, 1790–1797.
43 D.-C. Liu, D.-C. Zhong and T.-B. Lu, *EnergyChem*, 2020, **2**, 100034.
44 A. Touqeer, L. Shuang, S. Muhammad, L. Ke, A. Mohsin, L. Liang and C. Wei, *Nano Research Energy*, 2022, **1**, e9120021.
45 B. H. Weiyi Chen, C. Tian, X. Liu, S. Liang, H. Deng and Z. Lin, *Appl. Catal., B*, 2019, **244**, 996–1003.
46 X. Chang, T. Wang and J. Gong, *Energy Environ. Sci.*, 2016, **9**, 2177–2196.
47 K. Li, B. Peng and T. Peng, *ACS Catal.*, 2016, **6**, 7485–7527.
48 J. Schneider, H. Jia, J. T. Muckerman and E. Fujita, *Chem. Soc. Rev.*, 2012, **41**, 2036–2051.
49 X. Li, J. Wen, J. Low, Y. Fang and J. Yu, *Sci. China Mater.*, 2014, **57**, 70–100.
50 W. Zhang, A. R. Mohamed and W. J. Ong, *Angew. Chem., Int. Ed. Engl.*, 2020, **59**, 22894–22915.
51 R. Schlogl, *Angew. Chem., Int. Ed. Engl.*, 2015, **54**, 3465–3520.
52 A. Li, Q. Cao, G. Zhou, B. Schmidt, W. Zhu, X. Yuan, H. Huo, J. Gong and M. Antonietti, *Angew. Chem., Int. Ed. Engl.*, 2019, **58**, 14549–14555.
53 B. Pan, S. Luo, W. Su and X. Wang, *Appl. Catal., B*, 2015, **168–169**, 458–464.
54 A. Anzai, N. Fukuo, A. Yamamoto and H. Yoshida, *Catal. Commun.*, 2017, **100**, 134–138.
55 X. Cai, J. Wang, R. Wang, A. Wang, S. Zhong, J. Chen and S. Bai, *J. Mater. Chem. A*, 2019, **7**, 5266–5276.
56 Y. Zhao, Y. Wei, X. Wu, H. Zheng, Z. Zhao, J. Liu and J. Li, *Appl. Catal., B*, 2018, **226**, 360–372.
57 Y. Wang, Q. Lai, Y. He and M. Fan, *Catal. Commun.*, 2018, **108**, 98–102.
58 Z. Ma, P. Li, L. Ye, L. Wang, H. Xie and Y. Zhou, *Catal. Sci. Technol.*, 2018, **8**, 5129–5132.
59 W.-K. Jo, S. Kumar and S. Tonda, *Composites, Part B*, 2019, **176**, 107212.
60 B. Tahir, M. Tahir and N. A. Saidina Amin, *Mal. J. Fund. Appl. Sci.*, 2015, **11**, 114–117.
61 J. Jin, J. Luo, L. Zan and T. Peng, *Chemphyschem*, 2017, **18**, 3230–3239.
62 C. Lu, J. Li, J. Yan, B. Li, B. Huang and Z. Lou, *Appl. Mater. Today*, 2020, **20**, 100744.
63 X. Yang, S. Wang, N. Yang, W. Zhou, P. Wang, K. Jiang, S. Li, H. Song, X. Ding, H. Chen and J. Ye, *Appl. Catal., B*, 2019, **259**, 118088.
64 D. Jiang, W. Wang, E. Gao, S. Sun and L. Zhang, *Chem. Commun.*, 2014, **50**, 2005–2007.
65 R. Bhosale, S. Jain, C. P. Vinod, S. Kumar and S. Ogale, *ACS Appl. Mater. Interfaces*, 2019, **11**, 6174–6183.
66 Q. Shi, X. Zhang, Y. Yang, J. Huang, X. Fu, T. Wang, X. Liu, A. Sun, J. Ge, J. Shen, Y. Zhou and Z. Liu, *J. Energy Chem.*, 2021, **59**, 9–18.
67 Z. Wang, K. Teramura, Z. Huang, S. Hosokawa, Y. Sakata and T. Tanaka, *Catal. Sci. Technol.*, 2016, **6**, 1025–1032.
68 R. Chong, Y. Fan, Y. Du, L. Liu, Z. Chang and D. Li, *Int. J. Hydrogen Energy*, 2018, **43**, 22329–22339.
69 L. Zhao, F. Ye, D. Wang, X. Cai, C. Meng, H. Xie, J. Zhang and S. Bai, *ChemSusChem*, 2018, **11**, 3524–3533.
70 Y.-Y. Li, J.-S. Fan, R.-Q. Tan, H.-C. Yao, Y. Peng, Q.-C. Liu and Z.-J. Li, *ACS Appl. Mater. Interfaces*, 2020, **12**, 54507–54516.
71 W. Bi, Y. Hu, H. Jiang, L. Zhang and C. Li, *Adv. Funct. Mater.*, 2021, **31**, 2010780.
72 Y. Bai, P. Yang, L. Wang, B. Yang, H. Xie, Y. Zhou and L. Ye, *Chem. Eng. J.*, 2019, **360**, 473–482.
73 Q. Chen, X. Chen, M. Fang, J. Chen, Y. Li, Z. Xie, Q. Kuang and L. Zheng, *J. Mater. Chem. A*, 2019, **7**, 1334–1340.
74 S. Gao, B. Gu, X. Jiao, Y. Sun, X. Zu, F. Yang, W. Zhu, C. Wang, Z. Feng, B. Ye and Y. Xie, *J. Am. Chem. Soc.*, 2017, **139**, 3438–3445.
75 P. Xia, M. Antonietti, B. Zhu, T. Heil, J. Yu and S. Cao, *Adv. Funct. Mater.*, 2019, **29**, 1900093.
76 Y. Liang, X. Wu, X. Liu, C. Li and S. Liu, *Appl. Catal., B*, 2022, **304**, 120978.
77 H. Zhao, J. Duan, Z. Zhang and W. Wang, *ChemCatChem*, 2021, **14**, e2021017.
78 Y. Wang, X. Liu, X. Han, R. Godin, J. Chen, W. Zhou, C. Jiang, J. F. Thompson, K. B. Mustafa, S. A. Shevlin, J. R. Durrant, Z. Guo and J. Tang, *Nat. Commun.*, 2020, **11**, 2531.
79 M. Ma, Z. Huang, R. Wang, R. Zhang, T. Yang, Z. Rao, W. Fa, F. Zhang, Y. Cao, S. Yu and Y. Zhou, *Green Chem.*, 2022, **24**, 8791–8799.
80 W. Zhang, M. Jiang, S. Yang, Y. Hu, B. Mu, Z. Tie and Z. Jin, *Nano Research Energy*, 2022, **1**, e9120033.
81 Y.-X. Pan, Z.-Q. Sun, H.-P. Cong, Y.-L. Men, S. Xin, J. Song and S.-H. Yu, *Nano Res.*, 2016, **9**, 1689–1700.
82 B. Han, X. Ou, Z. Zhong, S. Liang, H. Deng and Z. Lin, *Small*, 2020, **16**, 2002985.
83 D. Wu, L. Ye, H. Y. Yip and P. K. Wong, *Catal. Sci. Technol.*, 2017, **7**, 265–271.
84 P. Yang, Z. J. Zhao, X. Chang, R. Mu, S. Zha, G. Zhang and J. Gong, *Angew. Chem., Int. Ed. Engl.*, 2018, **57**, 7724–7728.
85 C. Dong, M. Xing and J. Zhang, *J. Phys. Chem. Lett.*, 2016, **7**, 2962–2966.
86 K. Song, S. Liang, X. Zhong, M. Wang, X. Mo, X. Lei and Z. Lin, *Appl. Catal., B*, 2022, **309**, 121232.
87 X. Liu, L. Ye, S. Liu, Y. Li and X. Ji, *Sci. Rep.*, 2016, **6**, 38474.
88 M. Li, L. Zhang, X. Fan, M. Wu, M. Wang, R. Cheng, L. Zhang, H. Yao and J. Shi, *Appl. Catal., B*, 2017, **201**, 629–635.
89 J. Mao, T. Peng, X. Zhang, K. Li, L. Ye and L. Zan, *Catal. Sci. Technol.*, 2013, **3**, 1253–1260.
90 P. Tao, S. Yao, F. Liu, B. Wang, F. Huang and M. Wang, *J. Mater. Chem. A*, 2019, **7**, 23512–23536.
91 J. Xiong, J. Di and H. Li, *J. Mater. Chem. A*, 2021, **9**, 2662–2677.
92 M. Ge, C. Cao, J. Huang, S. Li, Z. Chen, K.-Q. Zhang, S. S. Al-Deyab and Y. Lai, *J. Mater. Chem. A*, 2016, **4**, 6772–6801.

93 P. Li, Y. Zhou, W. Tu, R. Wang, C. Zhang, Q. Liu, H. Li, Z. Li, H. Dai, J. Wang, S. Yan and Z. Zou, *CrystEngComm*, 2013, **15**, 9855–9858.
94 Z. Zhao, J. Zhang, M. Lei and Y. Lum, *Nano Research Energy*, 2023, **2**, e9120044.
95 G. Chen, M. Guo, X. Li, W. Wang, F. Liu, C. Ning, G. Yuan, J. Chen, S. Deng and C. Liu, *IEEE Trans. Electron Devices*, 2022, **69**, 2430–2435.
96 C. Chen, B. R. Yang, G. Li, H. Zhou, B. Huang, Q. Wu, R. Zhan, Y. Y. Noh, T. Minari, S. Zhang, S. Deng, H. Sirringhaus and C. Liu, *Adv. Sci.*, 2019, **6**, 1801189.
97 Z. Xiong, Z. Lei, C.-C. Kuang, X. Chen, B. Gong, Y. Zhao, J. Zhang, C. Zheng and J. C. S. Wu, *Appl. Catal., B*, 2017, **202**, 695–703.
98 B. Pan, S. Luo, W. Su and X. Wang, *Appl. Catal., B*, 2015, **168–169**, 458–464.
99 Y. Dou, A. Zhou, Y. Yao, S. Y. Lim, J.-R. Li and W. Zhang, *Appl. Catal., B*, 2021, **286**, 119876.
100 M. Manzanares, C. Fàbrega, J. Oriol Ossó, L. F. Vega, T. Andreu and J. R. Morante, *Appl. Catal., B*, 2014, **150–151**, 57–62.
101 M. Tahir and N. S. Amin, *Appl. Catal., A*, 2013, **467**, 483–496.
102 J. An, T. Shen, W. Chang, Y. Zhao, B. Qi and Y.-F. Song, *Inorg. Chem. Front.*, 2021, **8**, 996–1004.
103 C. Han, Y. Lei, B. Wang and Y. Wang, *ChemSusChem*, 2018, **11**, 4237–4245.
104 I. H. Tseng and J. C. S. Wu, *Catal. Today*, 2004, **97**, 113–119.
105 K. Teramura, Z. Wang, S. Hosokawa, Y. Sakata and T. Tanaka, *Chemistry*, 2014, **20**, 9906–9909.
106 I. H. Tseng, J. C. S. Wu and H.-Y. Chou, *J. Catal.*, 2004, **221**, 432–440.
107 S. Feng, J. Zhao, Y. Bai, X. Liang, T. Wang and C. Wang, *J. CO_2 Util.*, 2020, **38**, 1–9.
108 D. Luo, Y. Bi, W. Kan, N. Zhang and S. Hong, *J. Mol. Struct.*, 2011, **994**, 325–331.
109 P. Devi and J. P. Singh, *J. CO2 Util.*, 2021, **43**, 101376.
110 W. Bi, Y. Hu, H. Jiang, L. Zhang and C. Li, *Adv. Funct. Mater.*, 2021, **31**, 2010780.
111 Y. X. Pan, Y. You, S. Xin, Y. Li, G. Fu, Z. Cui, Y. L. Men, F. F. Cao, S. H. Yu and J. B. Goodenough, *J. Am. Chem. Soc.*, 2017, **139**, 4123–4129.
112 Y. He, Y. Wang, L. Zhang, B. Teng and M. Fan, *Appl. Catal., B*, 2015, **168–169**, 1–8.
113 H. Shi, G. Chen, C. Zhang and Z. Zou, *ACS Catal.*, 2014, **4**, 3637–3643.
114 N. T. Thanh Truc, N. T. Hanh, M. V. Nguyen, N. T. P. Le Chi, N. Van Noi, D. T. Tran, M. N. Ha, D. Q. Trung and T.-D. Pham, *Appl. Surf. Sci.*, 2018, **457**, 968–974.
115 W. Yu, D. Xu and T. Peng, *J. Mater. Chem. A*, 2015, **3**, 19936–19947.
116 L. Liu, *Ceram. Int.*, 2016, **42**, 12516–12520.
117 Y. T. Liang, B. K. Vijayan, K. A. Gray and M. C. Hersam, *Nano Lett.*, 2011, **11**, 2865–2870.
118 J. Mao, T. Peng, X. Zhang, K. Li and L. Zan, *Catal. Commun.*, 2012, **28**, 38–41.
119 X. Y.-z. Zhao Lin, R. Chen and Y. Diao, *J. Synth. Cryst.*, 2018, **47**, 2663–2668.
120 S. K. Parayil, A. Razzaq, S.-M. Park, H. R. Kim, C. A. Grimes and S.-I. In, *Appl. Catal., A*, 2015, **498**, 205–213.
121 M. Z. Dandan Lu, Z. Zhang, Q. Li, X. Wang and J. Yang, *Nanoscale Res. Lett.*, 2014, **272**, 9.
122 X. Li, W. Bi, Z. Wang, W. Zhu, W. Chu, C. Wu and Y. Xie, *Nano Res.*, 2018, **11**, 3362–3370.
123 Q. Zhang, T. Gao, J. M. Andino and Y. Li, *Appl. Catal., B*, 2012, **123–124**, 257–264.
124 Q. Zhang, Y. Li, E. A. Ackerman, M. Gajdardziska-Josifovska and H. Li, *Appl. Catal., A*, 2011, **400**, 195–202.
125 Q. Liu, Q. Chen, T. Li, Q. Ren, S. Zhong, Y. Zhao and S. Bai, *J. Mater. Chem. A*, 2019, **7**, 27007–27015.
126 J. Pan, G. Liu, G. Q. Lu and H. M. Cheng, *Angew. Chem., Int. Ed. Engl.*, 2011, **50**, 2133–2137.
127 M. Lazzeri, A. Vittadini and A. Selloni, *Phys. Rev. B: Condens. Matter Mater. Phys.*, 2001, **63**, 155409.
128 J. Pan, X. Wu, L. Wang, G. Liu, G. Q. Lu and H. M. Cheng, *Chem. Commun.*, 2011, **47**, 8361–8363.
129 Y. Ma, X. Wang, Y. Jia, X. Chen, H. Han and C. Li, *Chem. Rev.*, 2014, **114**, 9987–10043.
130 J. Mao, L. Ye, K. Li, X. Zhang, J. Liu, T. Peng and L. Zan, *Appl. Catal., B*, 2014, **144**, 855–862.
131 B. Han, X. Ou, Z. Deng, Y. Song, C. Tian, H. Deng, Y. J. Xu and Z. Lin, *Angew. Chem., Int. Ed.*, 2018, **57**, 16811–16815.
132 X. Xiong, C. Mao, Z. Yang, Q. Zhang, G. I. N. Waterhouse, L. Gu and T. Zhang, *Adv. Energy Mater.*, 2020, **10**, 2002928.
133 L. Wang, B. Zhao, C. Wang, M. Sun, Y. Yu and B. Zhang, *J. Mater. Chem. A*, 2020, **8**, 10175–10179.
134 H. Pang, X. Meng, P. Li, K. Chang, W. Zhou, X. Wang, X. Zhang, W. Jevasuwan, N. Fukata, D. Wang and J. Ye, *ACS Energy Lett.*, 2019, **4**, 1387–1393.
135 A. K. Kharade and S.-m. Chang, *J. Phys. Chem. C*, 2020, **124**, 10981–10992.
136 T. Billo, F. Y. Fu, P. Raghunath, I. Shown, W. F. Chen, H. T. Lien, T. H. Shen, J. F. Lee, T. S. Chan, K. Y. Huang, C. I. Wu, M. C. Lin, J. S. Hwang, C. H. Lee, L. C. Chen and K. H. Chen, *Small*, 2018, **14**, 1702928.
137 X. Zhang, Z. Zhang, J. Li, X. Zhao, D. Wu and Z. Zhou, *J. Mater. Chem. A*, 2017, **5**, 12899–12903.
138 P. Huang, J. Huang, S. A. Pantovich, A. D. Carl, T. G. Fenton, C. A. Caputo, R. L. Grimm, A. I. Frenkel and G. Li, *J. Am. Chem. Soc.*, 2018, **140**, 16042–16047.
139 X. Qian, W. Yang, S. Gao, J. Xiao, S. Basu, A. Yoshimura, Y. Shi, V. Meunier and Q. Li, *ACS Appl. Mater. Interfaces*, 2020, **12**, 55982–55993.
140 Q. Lang, W. Hu, P. Zhou, T. Huang, S. Zhong, L. Yang, J. Chen and S. Bai, *Nanotechnology*, 2017, **28**, 484003.
141 C. Han, Y. Lei, B. Wang, C. Wu, X. Zhang, S. Shen, L. Sun, Q. Tian, Q. Feng and Y. Wang, *Chem. Commun.*, 2019, **55**, 1572–1575.
142 M. Ye, X. Wang, E. Liu, J. Ye and D. Wang, *ChemSusChem*, 2018, **11**, 1606–1611.
143 Y. Peng, L. Wang, Q. Luo, Y. Cao, Y. Dai, Z. Li, H. Li, X. Zheng, W. Yan, J. Yang and J. Zeng, *Chem*, 2018, **4**, 613–625.

144 J. Di, C. Chen, C. Zhu, P. Song, J. Xiong, M. Ji, J. Zhou, Q. Fu, M. Xu, W. Hao, J. Xia, S. Li, H. Li and Z. Liu, *ACS Appl. Mater. Interfaces*, 2019, **11**, 30786–30792.
145 Y. Liu, B. Huang, Y. Dai, X. Zhang, X. Qin, M. Jiang and M.-H. Whangbo, *Catal. Commun.*, 2009, **11**, 210–213.
146 X. Zhu, A. Yamamoto, S. Imai, A. Tanaka, H. Kominami and H. Yoshida, *Appl. Catal., B*, 2020, **274**, 119085.
147 P. Li, Y. Zhou, Z. Zhao, Q. Xu, X. Wang, M. Xiao and Z. Zou, *J. Am. Chem. Soc.*, 2015, **137**, 9547–9550.
148 Q. Han, X. Bai, Z. Man, H. He, L. Li, J. Hu, A. Alsaedi, T. Hayat, Z. Yu, W. Zhang, J. Wang, Y. Zhou and Z. Zou, *J. Am. Chem. Soc.*, 2019, **141**, 4209–4213.
149 C. Gao, Q. Meng, K. Zhao, H. Yin, D. Wang, J. Guo, S. Zhao, L. Chang, M. He, Q. Li, H. Zhao, X. Huang, Y. Gao and Z. Tang, *Adv. Mater.*, 2016, **28**, 6485–6490.
150 C. Gao, Q. Meng, K. Zhao, H. Yin, D. Wang, J. Guo, S. Zhao, L. Chang, M. He, Q. Li, H. Zhao, X. Huang, Y. Gao and Z. Tang, *Adv. Mater.*, 2016, **28**, 6485–6490.